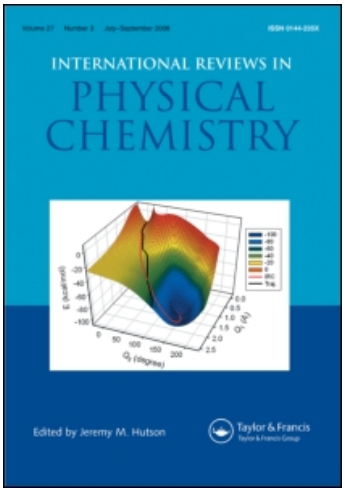

International Reviews in Physical Chemistry
Publication details, including instructions for authors and subscription information:
http://www.informaworld.com/smpp/title~content=t713724383

Calculating the energy spectra of magnetic molecules: application of real- and spin-space symmetries

Roman Schnalle[a]; Jürgen Schnack[a]
[a] Universität Bielefeld, Fakultät fär Physik, D-33501 Bielefeld, Germany

First published on: 02 July 2010

To cite this Article Schnalle, Roman and Schnack, Jürgen(2010) 'Calculating the energy spectra of magnetic molecules: application of real- and spin-space symmetries', International Reviews in Physical Chemistry, 29: 3, 403 — 452, First published on: 02 July 2010 (iFirst)
To link to this Article: DOI: 10.1080/0144235X.2010.485755
URL: http://dx.doi.org/10.1080/0144235X.2010.485755

International Reviews in Physical Chemistry
Vol. 29, No. 3, July–September 2010, 403–452

Taylor & Francis
Taylor & Francis Group

Calculating the energy spectra of magnetic molecules: application of real- and spin-space symmetries

Roman Schnalle* and Jürgen Schnack

Universität Bielefeld, Fakultät für Physik, Postfach 100131, D-33501 Bielefeld, Germany

(*Received 8 March 2010; final version received 12 April 2010*)

The determination of the energy spectra of small spin systems as for instance given by magnetic molecules is a demanding numerical problem. In this work we review numerical approaches to diagonalize the Heisenberg Hamiltonian that employ symmetries; in particular we focus on the spin-rotational symmetry $SU(2)$ in combination with point-group symmetries. With these methods one is able to block-diagonalize the Hamiltonian and thus to treat spin systems of unprecedented size. Thermodynamic observables such as the magnetization are then easily evaluated. In addition it provides a spectroscopic labeling by irreducible representations that can be related to selection rules which can be helpful when interpreting transitions induced by electron paramagnetic resonance, nuclear magnetic resonance or inelastic neutron scattering. It is our aim to provide the reader with detailed knowledge on how to set up such a diagonalization scheme.

Keywords: Heisenberg model; numerically exact energy spectrum; irreducible tensor operators; approximate diagonalization

Contents

*Corresponding author. Email: rschnall@uni-bielefeld.de

ISSN 0144–235X print/ISSN 1366–591X online

DOI: 10.1080/0144235X.2010.485755
http://www.informaworld.com

1. Introduction

Magnetism is a research field that is almost as old as human writing. It took several thousand years until its nature, which is quantum, could be determined. In 1928 Werner Heisenberg published his work on the theory of ferromagnetism, *Zur Theorie des Ferromagnetismus*, in which he introduced what is today called the Heisenberg model [1]. That this spin-only model is successfully applicable to magnetism rests on the property of many iron group elements to possess a quenched angular momentum in chemical compounds [2]. Therefore, for many magnetic substances the Heisenberg Hamiltonian provides the dominant term whereas effects connected to spin–orbit interaction are treated perturbatively in these systems. For theoretical work on non-Heisenberg systems see e.g. Refs. [3–7].

The Heisenberg Hamiltonian

$$\underset{\sim}{H}_{\mathrm{Heisenberg}} = -\sum_{i,j} J_{ij}\underset{\sim}{\mathbf{s}}(i)\cdot\underset{\sim}{\mathbf{s}}(j) \tag{1}$$

models the magnetic system by a sum of pairwise interactions between spins. The interaction strength (exchange parameter) between spins at sites i and j is given by a number J_{ij} with $J_{ij}<0$ referring to an antiferromagnetic and $J_{ij}>0$ to a ferromagnetic coupling. The spins are described by vector operators.

In order to understand magnetic observables such as magnetization, susceptibility, heat capacity, or electron paramagnetic resonance (EPR), nuclear magnetic resonance (NMR) and inelastic neutron scattering (INS) spectra the knowledge of the full energy spectrum of the investigated small magnetic system as for instance a magnetic molecule is often indispensable. Although the Heisenberg Hamiltonian, Equation (1), appears to be not too complicated, analytical solutions are known only for very small numbers of spins [8–10] or for instance for the spin-1/2 chain via the Bethe ansatz [11]. The attempt to diagonalize the Hamilton matrix numerically is very often severely restricted due to the huge dimension of the underlying Hilbert space. For a magnetic system of N spins of spin quantum number s the dimension is $(2s+1)^N$ which grows exponentially with N.

Group-theoretical methods can help to ease this numerical problem. A further benefit is given by the characterization of the obtained energy levels by quantum numbers and the classification according to irreducible representations. This review intends to provide an overview of the latest developments in efficient numerical diagonalization techniques of the Heisenberg model using symmetries. In particular we focus on the spin-rotational symmetry $SU(2)$ in combination with point-group symmetries.

The full rotational symmetry of angular momenta has been employed for quite a while. In quantum chemistry the method of irreducible tensor operators was adapted to few spin systems along with the upcoming field of molecular magnetism [12–17]. Nowadays the computer program *MAGPACK*, which completely diagonalizes the Heisenberg Hamiltonian using $SU(2)$ symmetry, is freely available [18]. Also for the approximate determination of energy eigenvalues by means of Density Matrix Renormalization Group (DMRG) methods [19,20], which can for instance treat chains of a few hundreds of spins with high accuracy, spin-rotational symmetry was employed [21]. In other fields such as nuclear physics this method was also adapted to model finite Fermi systems such as nuclei employing $SU(2)$ symmetry [22]. Early applications are also known for Hubbard models, where one can actually exploit two $SU(2)$ symmetries [23–26].

Besides spin-rotational symmetry many magnetic molecules or spin lattices possess spatial symmetries that can be expressed as point-group symmetries. Nevertheless, a combination of $SU(2)$ with point-group symmetries is not very common. The reason, as will become more apparent later, is that a rearrangement of spins due to point-group operations easily leads to complicated basis transformations between different coupling schemes. A possible compromise is to use only part of the spin-rotational symmetry (namely rotations about the z-axis) together with point-group symmetries [27–30] or to expand all basis states in terms of simpler product states [31–33]. During the past years a few attempts have been undertaken to combine the full spin-rotational symmetry with point-group symmetries. Oliver Waldmann combines the full spin-rotational symmetry with those point-group symmetries that are compatible with the spin coupling scheme, i.e. avoiding complicated basis transformations between different coupling schemes [34]. Along the same lines, especially low-symmetry groups such as D_2 are often applicable since the coupling scheme can be organized accordingly, compare Ref. [35] for an early investigation. Sinitsyn, Bostrem, and Ovchinnikov follow a similar route for the square lattice antiferromagnet by employing D_4 point-group symmetry [36,37].

Very recently a general scheme was developed that allows us to combine spin-rotational symmetry with general point-group symmetries [38–40]. The key problem, that the application of point-group operations leads to states belonging to a basis characterized by a different coupling scheme whose representation in the original basis is not (easily) known, can be solved by means of graph-theoretical methods that have been developed in another context [41,42]. We discuss in detail how this method can be implemented and present results for numerical exact diagonalizations of Heisenberg spin systems of unprecedented size [39,40,43,44]. Our aim is to provide the reader with sufficient material to be able to employ these powerful group-theoretical methods. They can for instance also be applied to calculate higher order Wigner-nJ symbols that appear when the double exchange is modeled in mixed-valent spin systems [45–47].

The article is organized as follows. Section 2 introduces the basic concepts, i.e. the Hamiltonian and its properties, the irreducible tensor operators, point group operations,

and the construction of basis states for irreducible representations. Section 3 demonstrates with the help of three examples that the Hamiltonian of spin systems of unprecedented size can be diagonalized completely. The outlook in Section 4 briefly summarizes and shows perspectives. The main part of this article is contained in an extended appendix that explains all the technical details to set up the discussed diagonalization scheme.

2. Conceptual ideas

2.1. *Spin Hamiltonian of magnetic molecules*

The research field of molecular magnetism deals with the investigation of the magnetic properties of chemical compounds composed of a number of ions that reaches from only a few up to dozens of them [48–51]. For the magnetic modeling of the molecule only those ions are taken into account which possess unpaired electrons and thus a non-vanishing magnetic moment. Since the molecules, which are prepared in the form of a crystal or powder sample, are often quite well separated from each other by their ligands, intermolecular interactions can be neglected in most cases. Additionally, the electrons can very often be treated as localized so that both features lead to a simplified sketch of the chemical compound, namely a spin system. The interactions between different spins of the system then depend of course on the chemical environment and stem from direct exchange or super-exchange [52] via chemical bridges. Figure 1 shows such a simplification for a Cr_8^{III} compound which can easily be modeled by a ring-like system of interacting spins [53–55].

A general Hamiltonian that models magnetic molecules could be written as

$$\underset{\sim}{H}_{\text{general}} = \underset{\sim}{H}_{\text{exchange}} + \underset{\sim}{H}_{\text{Zeeman}}, \tag{2}$$

where, to be more specific, in a system of N spins, i.e. $i, j = 1, \ldots, N$, the two terms assume the form

$$\underset{\sim}{H}_{\text{exchange}} = \sum_{i,j} \underset{\sim}{\mathbf{s}}(i) \cdot \mathbf{J}_{ij} \cdot \underset{\sim}{\mathbf{s}}(j), \tag{3}$$

$$\underset{\sim}{H}_{\text{Zeeman}} = \mu_B \sum_i \underset{\sim}{\mathbf{s}}(i) \cdot \mathbf{g}_i \cdot \vec{B}. \tag{4}$$

$\underset{\sim}{H}_{\text{exchange}}$ describes in a compact way the (isotropic and anisotropic) exchange interaction between two single-spin vector operators $\underset{\sim}{\mathbf{s}}(i)$ and $\underset{\sim}{\mathbf{s}}(j)$ as well as the single-ion anisotropy [14]. The quantity $\mathbf{J}_{ij}$ is a second-rank Cartesian tensor containing the corresponding parameters. $\underset{\sim}{H}_{\text{Zeeman}}$ couples the spins to an external magnetic field $\vec{B}$. In general, the coupling to an external field can be anisotropic and is thus described by local matrices $\mathbf{g}_i$.

It turns out that for many magnetic molecules the isotropic Heisenberg Hamilton operator provides a very good model. This means that anisotropic contributions can be neglected, as will be done in the following. In addition, we assume that for the highly symmetric spin systems to be treated in this article $\mathbf{g}_i = g$ are scalars, and the same

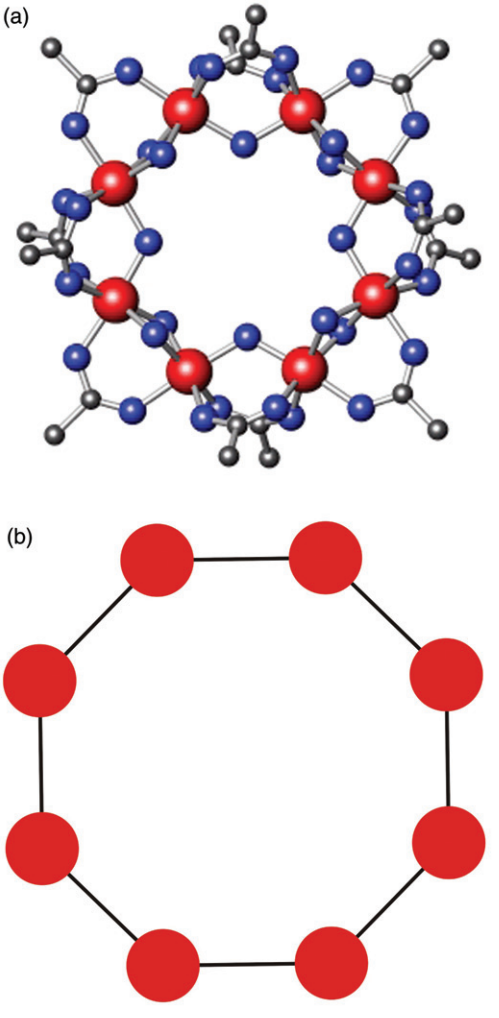

Figure 1. [Colour online] Simplification of the chemical structure of a Cr_8^{III} compound (top) to the corresponding spin system for the same molecule (bottom). Dots represent spin sites, lines exchange interactions.

for all ions. Then the resulting Hamiltonian that models the system simplifies to

$$\underset{\sim}{H} = \underset{\sim}{H}_{\text{Heisenberg}} + \underset{\sim}{H}_{\text{Zeeman}} \tag{5}$$

with

$$\underset{\sim}{H}_{\text{Heisenberg}} = -\sum_{i,j} J_{ij} \underset{\sim}{\mathbf{s}}(i) \cdot \underset{\sim}{\mathbf{s}}(j) \tag{6}$$

$$\underset{\sim}{H}_{\text{Zeeman}} = g\mu_B \underset{\sim}{\mathbf{S}} \cdot \vec{B}. \tag{7}$$

where $\underset{\sim}{\mathbf{S}} = \sum_i \underset{\sim}{\mathbf{s}}(i)$ is the total spin. As already mentioned, $J_{ij}<0$ refers to an antiferromagnetic and $J_{ij}>0$ to a ferromagnetic coupling.

The Heisenberg Hamiltonian is completely isotropic in spin space ($SU(2)$ symmetry), i.e. the commutators of the square of the total spin $\underset{\sim}{\mathbf{S}}$ and its z-component $\underset{\sim}{S}^z$ with $\underset{\sim}{H}_{\text{Heisenberg}}$ vanish

$$\left[\underset{\sim}{H}_{\text{Heisenberg}}, \underset{\sim}{S}^z\right] = 0, \quad \left[\underset{\sim}{H}_{\text{Heisenberg}}, \underset{\sim}{\mathbf{S}}^2\right] = 0. \tag{8}$$

Since $\left[\underset{\sim}{\mathbf{S}}^2, \underset{\sim}{S}^z\right] = 0$, the total magnetic quantum number M and the quantum number of the total spin S serve as good quantum numbers and a simultaneous eigenbasis of $\underset{\sim}{S}^z$, $\underset{\sim}{\mathbf{S}}^2$ and $\underset{\sim}{H}_{\text{Heisenberg}}$ can be found.

A well adapted basis is then given by states of the form $|\alpha SM\rangle$ which can be constructed according to a vector-coupling scheme (see Appendix A.2). These states are already orthogonal eigenstates of $\underset{\sim}{\mathbf{S}}^2$ and $\underset{\sim}{S}^z$ and α denotes a set of additional quantum numbers resulting from the coupling of the single spins $\underset{\sim}{\mathbf{s}}(i)$ to the total spin $\underset{\sim}{\mathbf{S}}$. Due to Equations (8) the matrix elements of the Heisenberg Hamiltonian $\langle \alpha' S' M' | \underset{\sim}{H}_{\text{Heisenberg}} | \alpha SM \rangle$ between states with different S and M vanish, leading to a block-factorized Hamilton matrix in which each block can be diagonalized separately. In this case the field dependence of the energies induced by the Zeeman term in Equation (7) can easily be added without further complicated calculations. This is because the z-direction can be chosen to point along the external field, so that the Zeeman term commutes with $\underset{\sim}{H}_{\text{Heisenberg}}$, $\underset{\sim}{\mathbf{S}}^2$ and $\underset{\sim}{S}^z$. Then M still serves as a good quantum number, and the effect of the external field $\vec{B} = B \cdot \vec{e}^{\,z}$ on eigenstates of $\underset{\sim}{H}_{\text{Heisenberg}}$ results in a simple field dependence of the energy eigenvalues E_i according to

$$E_i(B) = E_i + g\mu_B B M_i. \tag{9}$$

This way thermodynamic properties depending on the temperature T and the external magnetic field $\vec{B}$ can easily be calculated from the energy spectrum of the investigated magnetic molecule once the energies E_i are known.

2.2. *Irreducible tensor operator method*

The determination of the matrix elements of the Heisenberg Hamiltonian can elegantly be achieved with the help of irreducible tensor operators [12–17]. To this end, it is necessary to reformulate the spin vector operators in terms of irreducible tensor operators and to subsequently use tensorial algebra. In this regard the underlying theory is clearly based on group as well as representation theory. At this point it would probably not make sense to introduce all group-theoretical tools which lead to a complete understanding of the technical implementations used in this work. Several textbooks provide deep knowledge about these topics and the authors would like to refer to those [56–61]. Nevertheless, at least the origin of the concepts and formulations shall be explained. Some understanding of abstract group and representation theory is assumed.

2.2.1. *Irreducible tensor operators*

An irreducible tensor operator $\underset{\sim}{\mathbf{T}}^{(k)}$ of rank k is defined by the transformation properties of its components q under a general coordinate rotation R according to

$$\underset{\sim}{D}(R)\underset{\sim}{T}{}^{(k)}_{q}\underset{\sim}{D}{}^{-1}(R) = \sum_{q'} \underset{\sim}{T}{}^{(k)}_{q'} D^{(k)}_{qq'}(R). \tag{10}$$

Here $\underset{\sim}{D}(R)$ denotes the operator associated with the coordinate rotation R. The subscripts q as well as q' take the values $-k, -k+1, \ldots, k$. The matrix elements of the so-called *Wigner rotation matrices* $\mathbf{D}^{(k)}(R)$ are denoted by $D^{(k)}_{qq'}(R)$ (cf. Appendix A.1).

The case $k = 0$ in Equation (10) directly leads to what is called a *scalar operator*. As can easily be seen, a scalar operator is invariant under coordinate rotation, i.e. with $D^{(0)}_{00}(R) = 1$

$$\begin{aligned} \underset{\sim}{D}(R)\underset{\sim}{T}{}^{(0)}\underset{\sim}{D}{}^{-1}(R) &= \underset{\sim}{T}{}^{(0)} D^{(0)}_{00}(R) \\ &= \underset{\sim}{T}{}^{(0)}. \end{aligned} \tag{11}$$

In analogy to the states which span the irreducible representation $D^{(1)}$ of R_3 and which are said to behave under coordinate rotations like the components of a vector the irreducible tensor operator $\underset{\sim}{\mathbf{T}}^{(1)}$ is called a *vector operator*. For example, the components of a first-rank irreducible tensor operator $\underset{\sim}{\mathbf{s}}^{(1)}$ derived from the Cartesian components of the spin vector operator are given by

$$\begin{aligned} \underset{\sim}{s}{}^{(1)}_{0} &= \underset{\sim}{s}{}^{z}, \\ \underset{\sim}{s}{}^{(1)}_{\pm 1} &= \mp\sqrt{\frac{1}{2}}\left(\underset{\sim}{s}{}^{x} \pm i\underset{\sim}{s}{}^{y}\right). \end{aligned} \tag{12}$$

Stressing the analogy between the behavior of states and irreducible tensor operators under coordinate rotations, the role of the components $\underset{\sim}{T}{}^{(k)}_{q}$ in Equation (10) has to be specified. The components of the irreducible tensor operator $\underset{\sim}{\mathbf{T}}^{(k)}$ of rank k serve as a basis and therefore span the $(2k+1)$-dimensional irreducible representation $D^{(k)}$ of the rotation group R_3.

For comparison, consider a group $\mathcal{G}$ and its irreducible representations $\Gamma(\mathcal{G})$. The direct product of the irreducible representations $\Gamma^{(i)}$ and $\Gamma^{(j)}$ separately spanned by two sets of basis vectors is given by $\Gamma^{(i)} \otimes \Gamma^{(j)}$. It is reducible (cf. Equation (32)) if linear combinations of the product functions can be found which transform as basis functions for an irreducible representation. This concept can – in a one-to-one correspondence – be extended to tensor operators since they behave like the above mentioned functions. As a result, the direct product of two irreducible tensor operators spanning $D^{(k_1)}$ and $D^{(k_2)}$ can be decomposed into irreducible representations spanned by linear combinations of the products $\underset{\sim}{T}{}^{(k_1)}_{q_1}\underset{\sim}{T}{}^{(k_2)}_{q_2}$. The coefficients of these linear combinations are the Clebsch–Gordan coefficients of Equation (34).

Formally, the direct product of two irreducible tensor operators is given by

$$\left\{\underset{\sim}{\mathbf{T}}^{(k_1)} \otimes \underset{\sim}{\mathbf{T}}^{(k_2)}\right\}^{(k)}_{q} = \sum_{q_1, q_2} C^{k_1\, k_2\, k}_{q_1\, q_2\, q}\, \underset{\sim}{T}{}^{(k_1)}_{q_1}\underset{\sim}{T}{}^{(k_2)}_{q_2}, \tag{13}$$

where possible values of the resulting rank k can be determined in analogy to the vectorial coupling of spins and are given by $k = |k_1 - k_2|, |k_1 - k_2| + 1, \ldots, k_1 + k_2$. Equation (13) is a fundamental expression for the application of the irreducible tensor operator method within a numerical exact diagonalization routine. It leads to the desired formulation of the spin Hamiltonian in terms of irreducible tensor operators.

As an example, the coupling of the first-rank irreducible tensor operators $\underset{\sim}{\mathbf{U}}^{(1)}$ and $\underset{\sim}{\mathbf{V}}^{(1)}$ according to Equation (13) shall be presented here. Considering a compound irreducible tensor operator with $k = 0$, the coupling results in

$$\left\{\underset{\sim}{\mathbf{U}}^{(1)} \otimes \underset{\sim}{\mathbf{V}}^{(1)}\right\}^{(0)} = \frac{1}{\sqrt{3}}\left(\underset{\sim}{U}{}^{(1)}_{1}\underset{\sim}{V}{}^{(1)}_{-1} - \underset{\sim}{U}{}^{(1)}_{0}\underset{\sim}{V}{}^{(1)}_{0} + \underset{\sim}{U}{}^{(1)}_{-1}\underset{\sim}{V}{}^{(1)}_{1}\right), \tag{14}$$

where for the Clebsch–Gordan coefficients the equation $C^{110}_{q_1 q_2 0} = 1/\sqrt{3} \cdot (-1)^{1-q_1}\delta_{q_1, q_2}$ was used [62]. Expressing the spherical components of $\underset{\sim}{\mathbf{V}}^{(1)}$ and $\underset{\sim}{\mathbf{U}}^{(1)}$ in terms of the Cartesian components in analogy to Equation (12) yields

$$\left\{\underset{\sim}{\mathbf{U}}^{(1)} \otimes \underset{\sim}{\mathbf{V}}^{(1)}\right\}^{(0)} = -\frac{1}{\sqrt{3}}\left(\underset{\sim}{U}{}^{x}\underset{\sim}{V}{}^{x} + \underset{\sim}{U}{}^{y}\underset{\sim}{V}{}^{y} + \underset{\sim}{U}{}^{z}\underset{\sim}{V}{}^{z}\right), \tag{15}$$

which is, apart from the prefactor, the scalar product of the Cartesian vector operators $\underset{\sim}{\mathbf{U}}$ and $\underset{\sim}{\mathbf{V}}$.

Finally, the problem of coupling irreducible tensor operators is identical to the coupling of angular momenta (cf. Appendix A.1). Thus, from a mathematical point of view an advantage when using irreducible tensor operators is that one can adapt the mathematical approaches for coupling angular momenta and that one can refer to them.

2.2.2. *Matrix elements of irreducible tensor operators*

In the case of an irreducible tensor operator $\underset{\sim}{\mathbf{T}}^{(k)}$ the matrix elements of this operator can be calculated according to the *Wigner–Eckart theorem*. This states, for matrix elements with respect to spin states of the form $|\alpha S M\rangle$, that

$$\left\langle \alpha S M \middle| \underset{\sim}{T}{}^{(k)}_{q} \middle| \alpha' S' M' \right\rangle = (-1)^{S-M}\left\langle \alpha\, S \middle\| \underset{\sim}{\mathbf{T}}^{(k)} \middle\| \alpha'\, S' \right\rangle \begin{pmatrix} S & k & S' \\ -M & q & M' \end{pmatrix}. \tag{16}$$

The matrix element is apart from a phase factor decoupled into a Wigner-3J symbol and a quantity $\langle \alpha S \| \underset{\sim}{\mathbf{T}}^{(k)} \| \alpha' S' \rangle$ called the *reduced matrix element* of the irreducible tensor operator $\underset{\sim}{\mathbf{T}}^{(k)}$. The proof of Equation (16) is given in standard textbooks about group theory and quantum mechanics [56,61]. However, the physical meaning of this theorem and the consequences for the use within the irreducible tensor operator method shall be briefly discussed here.

First of all, it should be mentioned that the Wigner–Eckart theorem relies on the transformation properties of the wave functions and operators. Furthermore, since the reduced matrix element is completely independent of any magnetic quantum number, the Wigner–Eckart theorem separates the physical part of the matrix element – the reduced matrix element – from the purely geometrical part reflected by the Wigner-3J symbol. The value of the reduced matrix element depends on the particular form of the tensor operator and the states (cf. Appendix A.4) whereas the Wigner-3J symbol only depends on

rotational symmetry properties. If a zero-rank ($k=0$) irreducible tensor operator is assumed, the Wigner-3J symbol in Equation (16) directly reflects that there is no transition between states $|\alpha SM\rangle$ with different S or M. The matrix of the Heisenberg Hamiltonian from Equation (30), which can be written as a zero-rank irreducible tensor operator (see Appendix A.3), therefore takes block-diagonal form without further calculations.

According to Equation (16) the calculation of the matrix element of an irreducible tensor operator is directly related to the calculation of the reduced matrix element of this operator. The reduced matrix element of an irreducible tensor operator $\underset{\sim}{\mathbf{s}}^{(k)}$ with $k=0,1$, acting on a basis function of a single spin, can be derived from the evaluation of the Wigner–Eckart theorem. It yields the expressions

$$\langle s\|\underset{\sim}{\mathbf{s}}^{(0)}\|s\rangle = \langle s\|\underset{\sim}{\mathbf{1}}\|s\rangle = (2s+1)^{\frac{1}{2}}, \tag{17}$$

$$\langle s\|\underset{\sim}{\mathbf{s}}^{(1)}\|s\rangle = [s(s+1)(2s+1)]^{\frac{1}{2}}, \tag{18}$$

where the zero-rank irreducible tensor operator of a single spin $\underset{\sim}{\mathbf{s}}^{(0)}$ is given by the unity operator $\underset{\sim}{\mathbf{1}}$ and the components of $\underset{\sim}{\mathbf{s}}^{(1)}$ are given by Equation (12).

Using Equation (13) in combination with the Wigner–Eckart theorem in Equation (16) and a decomposition of states $|\alpha SM\rangle$ into product states according to Equation (34), one obtains the expression [63]

$$\begin{aligned}\langle \alpha_1 s_1 \alpha_2 s_2 S\|\left\{\underset{\sim}{\mathbf{T}}^{(k_1)}\otimes\underset{\sim}{\mathbf{T}}^{(k_2)}\right\}_q^{(k)}\|\alpha_1' s_1' \alpha_2' s_2' S'\rangle \\ = [(2S+1)(2S'+1)(2k+1)]^{\frac{1}{2}}\begin{pmatrix} s_1 & s_1' & k_1 \\ s_2 & s_2' & k_2 \\ S & S' & k\end{pmatrix} \\ \times \langle \alpha_1 s_1\|\underset{\sim}{\mathbf{T}}^{(k_1)}\|\alpha_1' s_1'\rangle\langle \alpha_2 s_2\|\underset{\sim}{\mathbf{T}}^{(k_2)}\|\alpha_2' s_2'\rangle.\end{aligned} \tag{19}$$

This is the reduced matrix element of a compound irreducible tensor operator of rank k which consists of the direct product of two irreducible tensor operators of general ranks k_1 and k_2.

Equation (19) is the basic formula for calculating reduced matrix elements of irreducible tensor operators composed of single-spin tensor operators as they appear in the Heisenberg Hamiltonian. By a successive application every irreducible tensor operator of that kind can be decoupled into a series of phase factors, Wigner-9J symbols and the reduced matrix elements of single-spin tensor operators (cf. Equation (12)). The successive application of Equation (19) is often called the *decoupling procedure* since the compound tensor operator that describes the system under consideration is decoupled so that its reduced matrix element can be calculated (see Appendix A.4).

2.3. *Point-group symmetries in Heisenberg spin systems*

Magnetic molecules, for instance those of Archimedian type [64–66], are often – not only from a scientific point of view – perceived to be of special beauty (cf. Figure 2). Certainly,

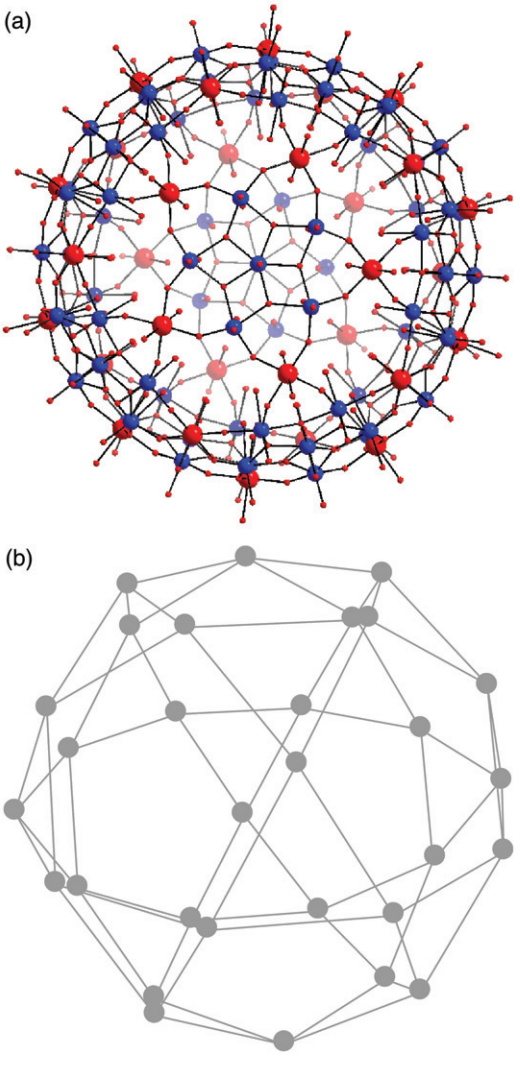

Figure 2. [Colour online] Sketch of the $\{Mo_{72}Fe_{30}\}$ molecule (top, picture taken from Ref. [65]). The underlying spin system exhibits the structure of an icosidodecahedron, i.e. possesses icosahedral (I_h) point-group symmetry (bottom).

this view is closely related to the high symmetry which can be found in the chemical structures and is referred to as point-group symmetry [67]. Point-group symmetries do not only contribute to the beauty of magnetic molecules, but they are also very instrumental in characterizing the energy levels of the spectra and thus in extracting physical information from the underlying spin system. Often a numerical exact diagonalization remains impossible unless point-group symmetries are used in order to reduce the dimensionalities of the Hamilton matrices.

It must be emphasized that there is a clear difference between a group of symmetry operations in real space that map the molecule on itself and the corresponding group of symmetry operations in a many-body spin system. Since from a physical point of view a magnetic molecule is described by a system of interacting spins with a certain coupling graph (cf. Figure 1(b)), the term point-group refers rather to a group of symmetry operations on this coupling graph than to operations in real space. As a direct result, the group-theoretical characterization is also rather based on the symmetry of the coupling graph than on the molecular symmetry. Of course, since the number of appearing coupling constants as well as their strengths are estimated from the chemical structure of the molecule, there is a close connection between the symmetries of the molecule and the corresponding coupling graph but not necessarily a one-to-one correspondence.

In Heisenberg spin systems point-group symmetries can be included by mapping the symmetry operations on spin permutations. In order to emphasize this, the term spin-permutational symmetry instead of point-group symmetry is often used. However, in the work at hand the term point-group symmetry is used although the symmetry is always incorporated by mapping the point-group operations on spin permutations. In context to this, it has to be mentioned that in systems which include anisotropies the incorporation of point-group symmetries is much more complicated since rotations in real space have to be performed [63,68–70].

Figure 3 exemplifies the coupling graphs of a square and a rectangle consisting of identical spins s with the symmetry axes of D_4 and D_2 being indicated. The rectangle can be seen as resulting from the square – a system of four interacting spins with only one coupling constant J – by introducing a second coupling constant of a different strength J' between spin pairs $\langle 1,4\rangle$ and $\langle 2,3\rangle$. In this case the coupling strength is indicated by the length of the coupling paths between the spins. The introduction of the second coupling constant then results in a reduction of the point-group symmetry from D_4 to D_2.

The point-group operations on the spin system can be identified with permutations of the spins that leave the Hamiltonian invariant [71]. Such a permutation is represented by

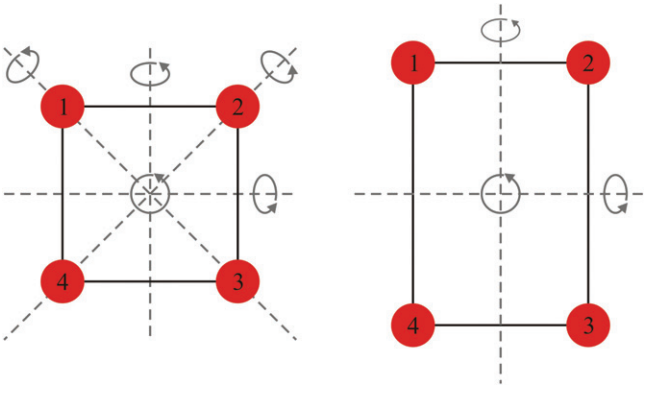

Figure 3. [Colour online] Coupling graph of a square of identical spins s with D_4 symmetry axes (left-hand side) and a rectangle with D_2 symmetry axes (right-hand side).

an operator $\underset{\sim}{G}(R_i)$ of the point-group $\mathcal{G}$ for which the commutation relation

$$\left[\underset{\sim}{H}_{\text{Heisenberg}}, \underset{\sim}{G}(R_i)\right] = 0 \tag{20}$$

holds, where $i = 1, \ldots, h$ numbers the symmetry operations up to the order h of $\mathcal{G}$.

The theory of group representations now provides the theoretical background for the use of point-group symmetries. The irreducible representations $\Gamma^{(n)}$ of a point-group $\mathcal{G}$ can be used to classify the energy eigenstates of $\underset{\sim}{H}_{\text{Heisenberg}}$ and to block-factorize the Hamilton matrices. The dimensionalities of the resulting subspaces, i.e. blocks, can be calculated with only little information. The irreducible matrix representations $\mathbf{\Gamma}^{(n)}(R_i)$ of the group elements, i.e. the permutation operators, are somewhat arbitrary concerning the choice of the underlying basis. Thus, these elements are represented by their character, i.e. the trace of the particular matrix representation. The character $\chi^{(n)}(R_i)$ is invariant under unitary transformations and is in general given by

$$\chi^{(n)}(R) = \text{Tr}\mathbf{\Gamma}^{(n)}(R) = \sum_{\lambda=1}^{l_n} \Gamma^{(n)}(R)_{\lambda\lambda}, \tag{21}$$

where l_n denotes the dimension of the n-th irreducible representation $\Gamma^{(n)}$.

A given character table of $\mathcal{G}$ now enables one to calculate the dimensions of the resulting blocks within the Hamilton matrix, i.e. the dimensions of the subspaces $\mathcal{H}(S, M, \Gamma^{(n)})$. Character tables for various point-groups can be found in almost every textbook about the theory of group representations. The authors would like to refer to [57,61,72] concerning the construction of character tables.

In order to calculate the dimensions of the subspaces $\mathcal{H}(S, M, \Gamma^{(n)})$, the reducible matrix representations $\mathbf{G}(R_i)$ of the operators $\underset{\sim}{G}(R_i)$ have to be considered. With $l, m = 1, \ldots, \dim \mathcal{H}(S, M)$ the matrix elements of these matrices are given by

$$G(R_i)_{lm} = \langle \alpha_l SM | \underset{\sim}{G}(R_i) | \alpha_m SM \rangle,$$

where the subscripts attached to α indicate that specific basis states are considered. The decomposition of the character $\chi(R_i) = \sum_{ll} G(R_i)_{ll}$ with respect to the irreducible representations n of $\mathcal{G}$ then yields

$$\chi(R_i) = \sum_n a_n \chi^{(n)}(R_i). \tag{22}$$

Using the great orthogonality theorem [61], the above equation results in the expression

$$\begin{aligned} a_n &= \dim \mathcal{H}(S, M, \Gamma^{(n)}) \\ &= \frac{1}{h} \sum_k N_k [\chi^{(n)}(\mathcal{C}_k)]^* \chi(\mathcal{C}_k), \end{aligned} \tag{23}$$

where a_n gives the multiplicity of the irreducible representation $\Gamma^{(n)}$ that is contained in the reducible representation $\mathbf{G}(\mathcal{C}_k)$. $\mathcal{C}$ refers to the classes which the group elements can be divided into. Each class contains equivalent operations, for example n-fold rotations, which are linked by the same group operation and thus hold the same character. N_k denotes the number of elements of $\mathcal{C}_k$.

From Equation (23) the dimensions of the subspaces $\mathcal{H}(S, M, \Gamma^{(n)})$ can be calculated, but no information about the basis states that span these Hilbert spaces is given. The required symmetrized basis states can be determined by the application of the projection operator [61]

$$\mathcal{P}^{(n)}_{\kappa\kappa} = \frac{l_n}{h} \sum_i [\Gamma^{(n)}(R_i)_{\kappa\kappa}]^* \underset{\sim}{G}(R_i). \tag{24}$$

This operator projects out that part of a function $|\phi\rangle$ which belongs to the κ-th row of the irreducible representation $\Gamma^{(n)}$. A subsequent application of the operator in Equation (24) on basis states, for example of the form $|\alpha SM\rangle$, is called the *basis-function generating machine* [61].

Although Equation (24) provides the information required to construct symmetrized basis states that serve as a basis for the irreducible representations of $\mathcal{G}$, it is important to notice that the matrices of $\Gamma^{(n)}$ have to be known completely. Of course, this does not cause a problem as long as $\mathcal{G}$ entirely consists of one-dimensional irreducible representations. However, if higher-dimensional irreducible representations appear, it is often more convenient to use the projection operator

$$\mathcal{P}^{(n)} = \sum_\kappa \mathcal{P}^{(n)}_{\kappa\kappa} = \frac{l_n}{h} \sum_i [\chi^{(n)}(R_i)]^* \underset{\sim}{G}(R_i), \tag{25}$$

which only requires information which can be extracted from the character table of $\mathcal{G}$. The operator of Equation (25) projects out that part of a function $|\alpha SM\rangle$ which belongs to the irreducible representation $\Gamma^{(n)}$, irrespective of the row. As a consequence one has to orthonormalize the resulting functions – for example by a *Gram–Schmidt orthonormalization* – in order to obtain the correct symmetrized basis functions (cf. Appendix A.5).

2.4. *Point-group symmetry operations acting on vector-coupling states*

In the previous Section 2.3 some general remarks about the use of point-group symmetries have already been made. In order to transform the Hamilton matrix to a block-diagonal form with respect to irreducible representations $\Gamma^{(n)}$ of a point group $\mathcal{G}$, one has to construct symmetrized basis functions $|\alpha SM\Gamma^{(n)}\rangle$. Equation (25) provides the projection operator that projects out that part of a state which belongs to the n-th irreducible representation of $\mathcal{G}$. However, the main challenge when constructing symmetrized basis states is to find an expression for the action of the operators $\underset{\sim}{G}(R_i)$ on states of the form $|\alpha SM\rangle$.

The above mentioned operators $\underset{\sim}{G}(R_i)$ which correspond to operations on the coupling graph (cf. Figure 3) can be defined by their action on the product basis composed of the single-spin eigenstates of $\underset{\sim}{s}^z(i)$. The states of the product basis of N identical spins can be denoted by

$$|s_1 m_1\rangle \otimes |s_2 m_2\rangle \otimes \cdots \otimes |s_N m_N\rangle \equiv |m_1 m_2 \cdots m_N\rangle$$

and fulfill the eigenvalue equation

$$\underset{\sim}{s}^z(i)|m_1 \cdots m_i \cdots m_N\rangle = m_i |m_1 \cdots m_i \cdots m_N\rangle$$

according to their definition.

Now, in a spin system consisting of N spins an operator $\underset{\sim}{G}(R)$ is considered that is given in the form $\underset{\sim}{G}(\pi(1)\pi(2)\cdots\pi(N))$ and describes a point-group operation. The notation $\underset{\sim}{G}(\pi)$ indicates for all $i=1,\ldots,N$ that the point-group operation interchanges the spin at site i with the spin at site $\pi(i)$. The action of the operator $\underset{\sim}{G}(R)$ on the product basis is given by

$$\underset{\sim}{G}(R)|m_1 m_2 \cdots m_N\rangle = |m_{\pi(1)}\, m_{\pi(2)} \cdots m_{\pi(N)}\rangle. \tag{26}$$

In Equation (26) the following happens: by the action of $\underset{\sim}{G}(R)$ the single-spin system at site i takes the z-component which the system at site $\pi(i)$ has taken previously. The result is a different state of the product basis with permuted m-values.

The operators $\underset{\sim}{G}(R)$ are only defined by their action on product states whereas the details of constructing symmetrized basis states that are linear combinations of vector-coupling states of the form $|\alpha SM\rangle$ are still unknown. How to find an expression for the action of $\underset{\sim}{G}(R)$ on these vector-coupling states is – to some extent – shown in Refs. [34] and [37].

However, a slightly different perspective concerned with the application of general symmetry operations to a vector-coupling basis shall be presented here (for further technical details see Appendix A.5). In order to clarify the action of an operator representing a point-group operation on a vector-coupling state, the states are labeled according to the coupling scheme they belong to. Additionally, the set of quantum numbers referring to the coupling scheme is abbreviated by Greek letters. Primes indicate different basis states within the same coupling scheme. With these conventions one obtains the following general result for a transition between two coupling schemes a and b which is induced by an operator $\underset{\sim}{G}$ representing a point-group operation:

$$\underset{\sim}{G}|\alpha SM\rangle_a = \delta_{\alpha,\beta}|\beta SM\rangle_b. \tag{27}$$

The Kronecker symbol $\delta_{\alpha,\beta}$ on the right-hand side indicates that the values of the spin quantum numbers of the different sets α and β are the same. Re-expressing the right-hand side of Equation (27) within states belonging to the coupling scheme a, i.e. inserting a suitable form of the identity operator $\underset{\sim}{\mathbf{1}}$, directly leads to the very important final result

$$\underset{\sim}{G}|\alpha SM\rangle_a = \sum_{\alpha'} \delta_{\alpha,\beta}\, {}_a\langle \alpha' SM|\beta SM\rangle_b\, |\alpha' SM\rangle_a \tag{28}$$

which contains so-called *general recoupling coefficients* ${}_a\langle \alpha SM|\beta SM\rangle_b$. A general recoupling coefficient can be seen as a scalar product between vector-coupling states belonging to different coupling schemes a and b.

It is by no means trivial to find an expression for a recoupling coefficient relating different coupling schemes if more than three or four spins are present. By definition the expressions for the elements of the transition matrix relating two different coupling schemes result in Wigner-nJ symbols (cf. Appendix A.1). While for three interacting spins Wigner-6J symbols occur, the size n of these Wigner coefficients increases with every additional spin taken into account. For four interacting spins the recoupling coefficient is expressed by a Wigner-9J symbol and for five interacting spins the recoupling is described by Wigner-12J symbols.

From a computational point of view it turns out to be unfavorable to use algebraic expressions for higher symbols than Wigner-9J symbols although there exist expressions

for 12J symbols and 15J symbols [62]. In order to find an effective way to describe general recoupling coefficients, one should use expressions in which only Wigner-6J symbols appear. These 6J symbols can be calculated using the formula [73]

$$\begin{Bmatrix} j_1 & j_2 & j_3 \\ J_1 & J_2 & J_3 \end{Bmatrix} = \Delta(j_1,j_2,j_3)\Delta(j_1,J_2,J_3) \times \Delta(J_1,j_2,J_3)\Delta(J_1,J_2,j_3)\sum_t \frac{(-1)^t(t+1)!}{f(t)}, \tag{29}$$

where the *triangle coefficient* $\Delta(a,b,c)$ reads

$$\Delta(a,b,c) = \left(\frac{(a+b-c)!\,(a-b+c)!\,(-a+b+c)!)}{(a+b+c+1)!}\right)^{\frac{1}{2}}.$$

The function $f(t)$ in Equation (29) is given by

$$\begin{aligned} f(t) = {} & (t-j_1-j_2-j_3)!\,(t-j_1-J_2-J_3)! \\ & \times (t-J_1-j_2-J_3)!\,(t-J_1-J_2-j_3)! \\ & \times (j_1+j_2+J_1+J_2-t)!\,(j_2+j_3+J_2+J_3-t)! \\ & \times (j_3+j_1+J_3+J_1-t)! \end{aligned}$$

The sum in Equation (29) runs over non-negative integer values of t for which no factorial in $f(t)$ has a negative argument. Since even the evaluation of Wigner-6J symbols is a rather involved task as can be seen from Equation (29), it is helpful to analyze the symmetry properties of the appearing symbols (cf. Figure 14 in the appendix) in order to reduce the computational effort when constructing symmetrized basis states. In this regard, when expressing the action of a point-group operation on a basis state according to Equation (28), only those recoupling coefficients have to be calculated which are non-zero.

So far, nothing has been said about the generation of a formula that describes a general recoupling coefficient. Finding a formula which only contains Wigner-6J symbols and some phase factors can most efficiently be done by using graph theory (see Appendix B). However, the choice of the coupling scheme which underlies the construction process of the basis states is essential for an effective computational realization of the numerical exact diagonalization. In this regard the invariance of the coupling scheme under the applied point-group operations is a desired property (see Appendices A.5 and A.6).

3. Applications

In this section we would like to present three applications for realistic spin systems of unprecedented size that can be treated using irreducible tensor operator techniques and point-group symmetries: a cuboctahedron of $N=12$ spins of spin quantum number $s=3/2$ (Hilbert space dimension 16,777,216), an icosahedron of $N=12$ spins of spin quantum number $s=3/2$ (same dimension), and a spin ring of $N=10$ and $s=5/2$ (Hilbert space dimension 60,466,176) known as the ferric wheel Fe_{10} [74].

It is very important to note that for the case of antiferromagnetic coupling the cuboctahedron as well as the icosahedron, see Figure 4, belong to the class of geometrically frustrated spin systems [40,75–77] and are thus hardly accessible by means

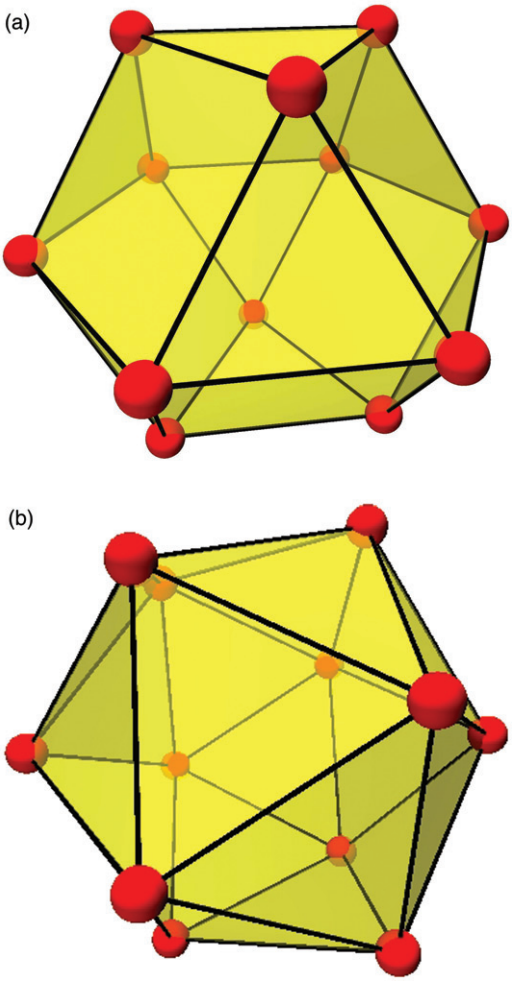

Figure 4. [Colour online] Structure of the cuboctahedron (top) and the icosahedron (bottom).

of Quantum Monte Carlo (QMC) calculations due to a so-called negative-sign problem [78–80]. Complete diagonalization is therefore the only way to study the interesting behavior of such systems both as functions of field and temperature [28,44,66,81].

Density Matrix Renormalization Group (DMRG) techniques provide a very powerful approximation mainly for one-dimensional spin systems such as chains [19,82,83]. The method delivers the relative ground states for orthogonal subspaces. Extensions to include the approximate evaluation of excitations have been developed recently [84], but are still primarily useful for one-dimensional systems. For the example of Fe_{10}, this method could provide lowest levels for each total magnetic quantum number M and thus one could evaluate the crossing fields of the lowest levels. More or less the same holds true for the Lanczos diagonalization technique [85], with which again extremal energy eigenvalues and eigenstates can be evaluated. Quantum Monte Carlo would be able to evaluate observables

for Fe_{10}, since this ten-site system is non-frustrated. Nevertheless, QMC cannot determine higher lying energy levels which would be crucial for, e.g. inelastic neutron scattering studies.

Since the three investigated systems exhibit a highly symmetric structure they can be modeled with just one nearest neighbor interaction, therefore the Heisenberg Hamiltonian simplifies to

$$\underset{\sim}{H}_{\text{Heisenberg}} = -J \sum_{\langle i,j \rangle} \underset{\sim}{\mathbf{s}}(i) \cdot \underset{\sim}{\mathbf{s}}(j). \tag{30}$$

The summation runs over pairs $\langle i, j \rangle$ of nearest neighbors of single-spin vector operators $\underset{\sim}{\mathbf{s}}$ at sites i and j counting each pair only once. For the following examples $J<0$ is assumed.

3.1. *The cuboctahedron*

The magnetism of antiferromagnetically coupled and geometrically frustrated spin systems is a fascinating subject due to the richness of phenomena that are observed [86,87]. One of the most famous spin systems is the two-dimensional kagomé lattice [87–92]. It is very interesting and from the point of view of theoretical modeling it is appealing that similar but zero-dimensional spin systems – in the form of magnetic molecules [64,65,93–95] – exist that potentially could show many of the special features of geometrically frustrated antiferromagnets. The cuboctahedron which consists of squares surrounded by triangles serves as one zero-dimensional "little brother" of the kagomé antiferromagnet; the icosidodecahedron, which consists of pentagons surrounded by triangles, is another one. Such finite size antiferromagnets offer the possibility to discover and understand properties that are shared by the infinitely extended lattices. An example is the discovery of localized independent magnons [91,96], which explain the unusual magnetization jump at the saturation field. Also the plateau at 1/3 of the saturation magnetization that appears in systems built of corner sharing triangles could be more deeply investigated by looking at the cuboctahedron and the icosidodecahedron [28,97].

The energy levels of the cuboctahedron ($N=12$, $s=3/2$, Hilbert space dimension 16,777,216), shown in Figure 5, could be numerically evaluated using the D_2 point-group symmetry. Since the Hamiltonian commutes with the total spin, the energy levels can be arranged in multiplets and plotted versus their total spin quantum number S. For symmetric spin systems with antiferromagnetic coupling the spectrum is usually bounded by parabolas [98–100].

For low-lying sectors of $S=0, 1, 2, 3$ we also determined the energy levels according to irreducible representations of the full octahedral group O_h, see Figure 6. One feature that can be clearly seen in Figure 6 is the existence of an additional low-lying singlet below the first triplet.

Figure 7 shows the magnetization curve at $T=0$ for the regular cuboctahedron with $s=3/2$. This curve shows the aforementioned plateau at 1/3 of the saturation magnetization and a jump to saturation of height $\Delta M=2$. This jump is insofar unusual since normally jumps in the magnetization curve occur at crossings of energy levels that belong to multiplets of adjacent total spin quantum numbers, i.e. 1 and 2 or 5 and 6. This always results in a jump of height one. If the jump is bigger it results from a crossing of levels whose spin quantum numbers have a difference bigger than one. Such a jump belongs to what is called frustration effects [44].

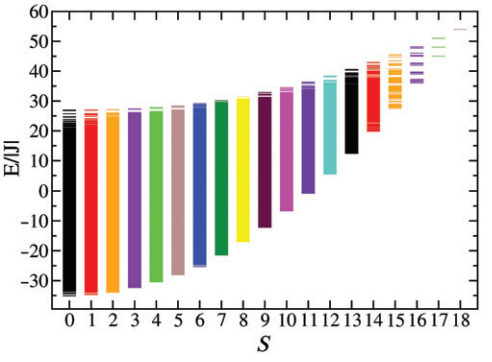

Figure 5. [Colour online] Full energy spectrum of a cuboctahedron with $s = 3/2$. The energy levels have been calculated using D_2 point-group symmetry. Since the Hamiltonian commutes with the total spin, the energy levels can be arranged in multiplets and plotted versus their total spin quantum number S.

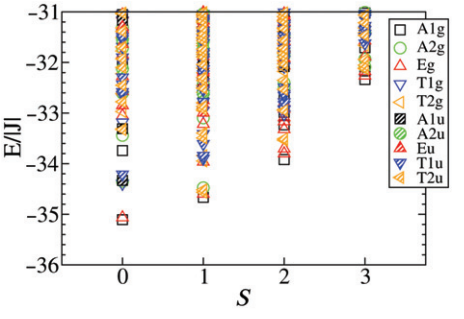

Figure 6. [Colour online] Low-lying part of the energy spectrum of a cuboctahedron $s = 3/2$. The energy levels are labeled according to irreducible representations of the full octahedral group O_h.

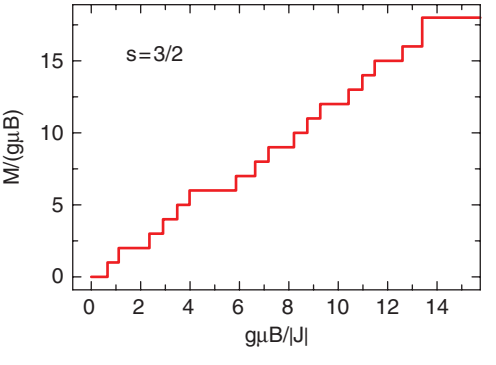

Figure 7. [Colour online] Magnetization as a function of applied field at $T = 0$ for the regular cuboctahedron with $s = 3/2$. The extended plateau at 1/3 of the saturation magnetization is clearly visible.

Figure 8 compares the heat capacity (top) and the zero-field susceptibility (bottom) for the regular cuboctahedron with $s = 1/2$, $s = 1$, and $s = 3/2$. The heat capacity shows a pronounced double peak structure for $s = 1/2$ and $s = 1$ which dissolves into a broad peak with increasing spin quantum number. The broad peak also moves to higher temperatures with increasing s. The reason for the first sharp peak is two-fold. Since there are several gaps between the low-lying levels the density of states has a very discontinuous structure which results in the double peak structure. For $s = 1/2$ the low-lying singlets provide a very low-lying non-magnetic density of states which is responsible for the fact that the first sharp peak is at such low temperatures. For $s = 1$ the first sharp peak results from both excited singlet as well as lowest triplet levels. For $s = 3/2$ a remnant of the first sharp peak is still visible; it is given by the low-lying singlets, but since they are so few, also influenced by the lowest triplet levels. The behavior of the heat capacity is contrasted by the susceptibility, bottom of Figure 8, which reflects mostly the density of states of magnetic levels and is only weakly influenced by low-lying singlets. Therefore, the first sharp peak, or any other structure at very low temperatures, is absent.

3.2. *The icosahedron*

A spin system where the spins are mounted at the vertices of an icosahedron and interact antiferromagnetically along the edges seems to be rather appealing since it exhibits unusual

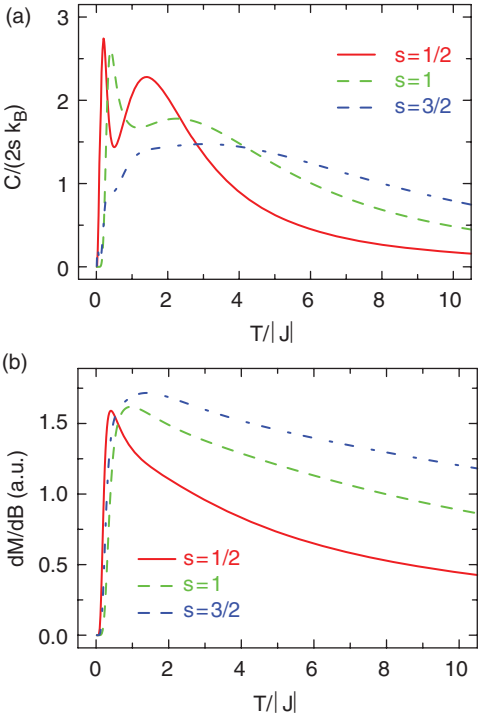

Figure 8. [Colour online] Zero-field heat capacity (top) and zero-field susceptibility (bottom) for the regular cuboctahedron with $s = 1/2$, $s = 1$, and $s = 3/2$.

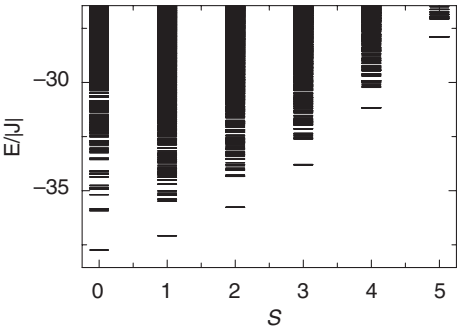

Figure 9. Low-lying energy levels of an antiferromagnetically coupled icosahedron $N = 12$ and $s = 3/2$. Since the Hamiltonian commutes with total spin, the energy levels can be arranged in multiplets and plotted versus their total spin quantum number S. The ground state possesses $S = 0$.

frustration properties such as metamagnetic phase transitions [76,101–103]. Unfortunately, it appears to be challenging to synthesize such structures although icosahedra are rather stable cluster configurations [104].

Here we investigate the properties of an icosahedron ($N = 12$) with single-spin quantum number $s = 3/2$ (Hilbert space dimension 16,777,216). The complete set of energy eigenvalues has been determined using D_2 symmetry. Figure 9 displays the low-lying part of all levels. Looking at the data file it turns out that very many (really unusually many) levels are highly degenerate, which is in accordance with earlier investigations of icosahedra with smaller single-spin quantum number [77,102]. We find that for every sector of total spin S and total magnetic quantum number M the irreducible representations A_2, B_1, and B_2 contain exactly the same energy eigenvalues, whereas A_1 is different. The non-degenerate ground state belongs to A_1. In addition very often near degeneracies occur.

Figure 10 shows the related zero-field heat capacity (top) and zero-field susceptibility (bottom). While the susceptibility does not look so unusual compared to other spin structures, the heat capacity appears to be really weird. Half way up the initial rise at very low temperatures there is a Schottky-like peak that stems from the slightly split ground state ($S = 0$) levels. The further rise is due to the fact that the lowest 2×3 degenerate ($S = 1$) level is energetically rather close. Although higher-lying levels are separated by gaps from the lowest levels they also contribute to the heat capacity due to their massive degeneracy. Altogether this results in a low-temperature heat capacity that strongly differs from the heat capacity of the cuboctahedron, cf. Figure 8.

The icosahedron may also serve as an example for the technical complexity due to the evaluation of recoupling coefficients. When combining I_h symmetry with $SU(2)$ many different recoupling formulas have to be generated (119 for the 120 group operations minus the identity to be precise). This renders a treatment of the $s = 3/2$ icosahedron in I_h impossible. Although the sizes of the Hamilton matrices for the irreducible representations would be small, it is the construction of basis states that turns the evaluation of the needed matrix elements into a very lengthy procedure. Even in a parallelized job on 256 cores on a supercomputer this task could not be completed. For the $s = 1$ icosahedron we could finish a decomposition into irreducible representations of I_h, but – to give an example – the

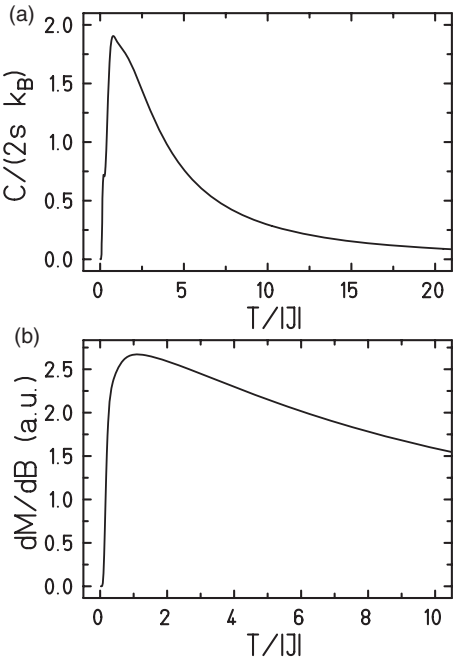

Figure 10. Zero-field heat capacity (top) and zero-field susceptibility (bottom) for the regular icosahedron with $s = 3/2$.

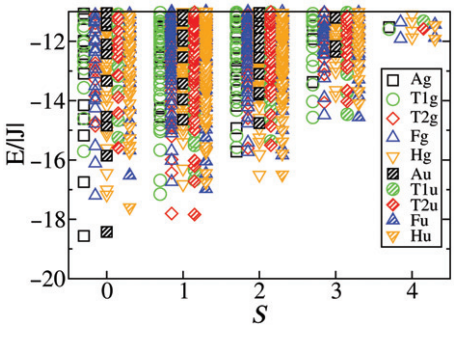

Figure 11. [Colour online] Low-lying part of the energy spectrum of an icosahedron with $s = 1$. The energy levels are labeled according to irreducible representations of the full icosahedral group I_h. Since the many symbols would overlap strongly they have been slightly displaced to improve clarity. Nevertheless, they belong to integer S values.

construction and subsequent diagonalization of the largest subspace, which has only a dimension of 3315, took about three days on 128 brand new Nehalem processors. Figure 11 shows the low-lying part of the energy spectrum of an icosahedron with $s = 1$. The energy levels are labeled according to irreducible representations of the full icosahedral group I_h. The exact and near degeneracies that have been discussed above

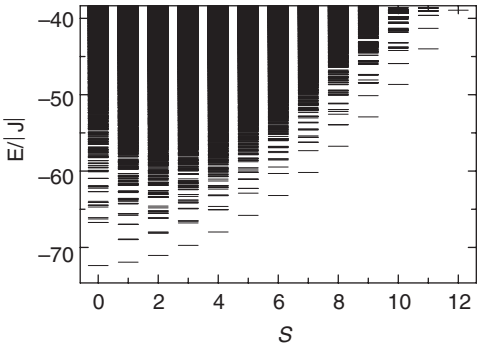

Figure 12. Low-lying energy levels of an antiferromagnetically coupled spin ring with $N = 10$ and $s = 5/2$. Since the Hamiltonian commutes with total spin, the energy levels can be arranged in multiplets and plotted versus their total spin quantum number S. The lowest energy eigenvalues $E_{\min}(S)$ obey an approximate quadratic dependence on total spin S (Landé's interval rule).

for the case of $s = 3/2$ and D_2 can now be resolved. For instance, the lowest $S = 1$ level belongs to T_{2u} and is thus three-fold degenerate. It is split from the higher-lying T_{2g} by only $3/1000|J|$, which in any calculation or measurement would look like a six-fold degeneracy, see also Ref. [102].

3.3. *Rings*

Molecular ferric wheels are among the very first magnetic molecules. It appears that they can be synthesized in many even numbered sizes, e.g. $N = 6, 8, \ldots, 18$ Fe^{III} spins [74,105–109]. Since the spin of the Fe(III) ions is $s = 5/2$ the Hilbert space dimension grows rapidly from one ring size to the next. For the ferric wheel Fe^{III}_{10} it already reaches 60,466,176 rendering a complete diagonalization impossible, at least in the past [74]. Based on the observation that the lowest energy eigenvalues $E_{\min}(S)$ obey a quadratic dependence with respect to total spin [39,43,110–113], which is Landé's interval rule, approximations could be derived for the level crossing fields [110] as well as for low-lying excitations in for instance the truly giant ferric wheel Fe^{III}_{18} [114]. As mentioned earlier, QMC is also capable of evaluating observables for even-membered unfrustrated spin rings [80]. Nevertheless, none of the methods is able to determine higher-lying states.

In the following we present the first complete diagonalization study of a spin ring similar to Fe^{III}_{10}, i.e. with $N = 10$ and $s = 5/2$. This enables us to subsequently evaluate all thermodynamic functions, all excited levels, and if needed even the evolution for time-dependent observables. For the diagonalization we used only the D_2 symmetry because it reduces the matrices already sufficiently and allows a faster computation of recoupling coefficients and thus matrix elements compared to the C_{10} symmetry.

Figure 12 displays the low-lying energy levels for various sectors of total spin S. The rotational band structure of energy levels, which is at the heart of the aforementioned approximation, is clearly visible. Having obtained the eigenvalues an evaluation of the magnetization as a function of temperature and field is easily possible. Figure 13 shows the susceptibility as a function of temperature (top) and the magnetization as a function of

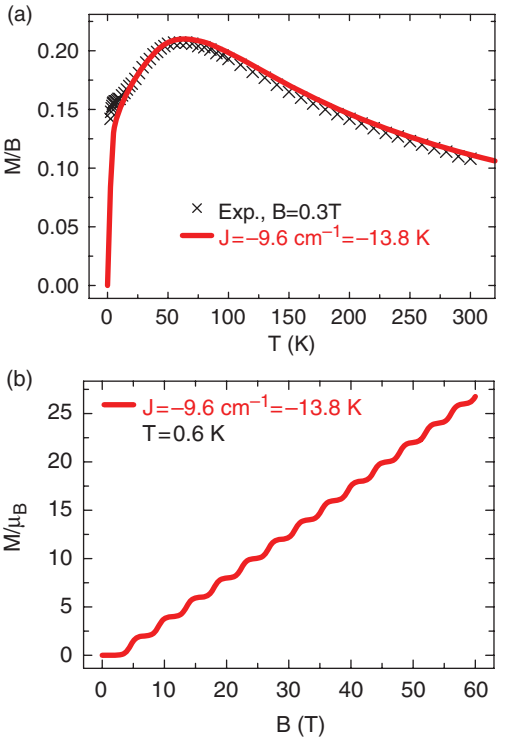

Figure 13. [Colour online] Susceptibility (top) and magnetization (bottom) of an antiferromagnetically coupled spin ring with $N=10$ and $s=5/2$. The exchange parameter $J=-9.6\,\mathrm{cm}^{-1}$ as well as the susceptibility data are taken from Ref. [74].

applied field (bottom) of an antiferromagnetically coupled spin ring with $N=10$ and $s=5/2$. The exchange parameter $J=-9.6\,\mathrm{cm}^{-1}$ as well as the susceptibility data are taken from Ref. [74]. $g=2.0$ was assumed for the calculation as in the original paper. Since the theoretical susceptibility curve is now known exactly, a detailed discussion of the experimental data becomes possible. As conjectured already in Ref. [74] the low-temperature hump of the susceptibility is not a feature of the ring Hamiltonian. We found numerically that it can also not be produced by a (reasonable) next-nearest neighbor interaction. The authors of the experimental paper suggested that it might be produced by dimers of Fe(III), that should also contribute (slightly) to the large temperature behavior, where the agreement with the theoretical curve is also not perfect. Our obtained energy eigenvalues would now allow us to set up a model that contains the ring and an unknown amount of dimer impurities. Open parameters would then be the amount of impurity and the g value which very likely deviates slightly from 2.

4. Outlook

In this review we have undertaken the attempt to explain how numerical approaches to diagonalize the Heisenberg Hamiltonian work, which employ the spin-rotational

symmetry $SU(2)$ in combination with point-group symmetries. We hope that we could provide the reader with detailed knowledge on how to set up such a diagonalization scheme, especially through the extended technical appendix.

What remains open for the future is to develop efficient schemes to evaluate recoupling coefficients, which at the present stage can be a very time consuming procedure that sometimes renders the calculation of matrix elements practically impossible although the complete matrix would be rather small in the end. A natural next step consists in finding optimal coupling schemes for a given molecule and point-group symmetry.

Acknowledgements

We thank Dante Gatteschi, Boris Tsukerblat, Martin Höck, and Jörg Ummethum for carefully reading the manuscript. This work was supported by the German Science Foundation (DFG) through the research group 945 and a Ph.D. program of the State of Lower Saxony at Osnabrück University. Computing time at the Leibniz Computing Center in Garching is also gratefully acknowledged. Last but not least we would like to thank the State of North Rhine-Westphalia and the DFG for financing our local SMP supercomputer as well as the companies BULL and ScaleMP for constant support.

References

[1] W. Heisenberg, Z. f. Phys. **49**, 619 (1928).
[2] C. Kittel, *Introduction to Solid State Physics* (John Wiley, New York, 2004).
[3] J. Borras-Almenar, J. Clemente-Juan, E. Coronado, A. Palii, and B. Tsukerblat, J. Phys. Chem. A **102**, 200 (1998).
[4] A. Ceulemans, L. Chibotaru, G. Heylen, K. Pierloot, and L. Vanquickenborne, Chem. Rev. **100**, 787 (2000).
[5] A. Palii, B. Tsukerblat, E. Coronado, J. Clemente-Juan, and J. Borras-Almenar, J. Chem. Phys. **118**, 5566 (2003).
[6] V. Mironov, L. Chibotaru, and A. Ceulemans, J. Am. Chem. Soc. **125**, 9750 (2003).
[7] A. Palii, B. Tsukerblat, J. M. Clemente-Juan, and E. Coronado, Int. Rev. Phys. Chem. **29**, 135 (2010).
[8] D. Kouzoudis, J. Magn. Magn. Mater. **173**, 259 (1997).
[9] D. Kouzoudis, J. Magn. Magn. Mater. **189**, 366 (1998).
[10] K. Bärwinkel, H.-J. Schmidt, and J. Schnack, J. Magn. Magn. Mater. **212**, 240 (2000).
[11] H. Bethe, Z. Phys. **71**, 205 (1931).
[12] D. Gatteschi and L. Pardi, Gazz. Chim. Ital. **123**, 231 (1993).
[13] J. J. Borras-Almenar, J. M. Clemente-Juan, E. Coronado, and B. S. Tsukerblat, Inorg. Chem. **38**, 6081 (1999).
[14] A. Bencini and D. Gatteschi, *Electron Paramagnetic Resonance of Exchange Coupled Systems* (Springer, Berlin, 1990).
[15] B. S. Tsukerblat, *Group Theory in Chemistry and Spectroscopy: A Simple Guide to Advanced Usage*, 2nd ed (Dover Publications, Mineola, New York, 2006).
[16] B. Tsukerblat, Inorg. Chim. Acta **361**, 3746 (2008).
[17] A. S. Boyarchenkov, I. G. Bostrem, and A. S. Ovchinnikov, Phys. Rev. B **76**, 224410 (2007).
[18] J. J. Borras-Almenar, J. M. Clemente-Juan, E. Coronado, and B. S. Tsukerblat, J. Comp. Chem. **22**, 985 (2001).
[19] S. R. White, Phys. Rev. B **48**, 10345 (1993).
[20] S. R. White and D. Huse, Phys. Rev. B **48**, 3844 (1993).

[21] I. P. McCulloch and M. Gulacsi, Europhys. Lett. **57**, 852 (2002).
[22] J. Dukelsky and S. Pittel, Rep. Prog. Phys. **67**, 513 (2004).
[23] I. Affleck, Z. Zou, T. Hsu, and P. Anderson, Phys. Rev. B **38**, 745 (1988).
[24] S. Zhang, Int. J. Mod. Phys. B **5**, 153 (1991).
[25] P. Lee, N. Nagaosa, T. Ng, and X. Wen, Phys. Rev. B **57**, 6003 (1998).
[26] R. Schumann, Ann. Phys.-Berlin **11**, 49 (2002).
[27] H. Schulz, T. Ziman, and D. Poilblanc, J. Phys. I **6**, 675 (1996).
[28] I. Rousochatzakis, A. M. Läuchli, and F. Mila, Phys. Rev. B **77**, 094420 (2008).
[29] J. Richter, J. Schulenburg, A. Honecker, and D. Schmalfuss, Phys. Rev. B **70**, 174454 (2004).
[30] J. Richter and J. Schulenburg, Eur. Phys. J. B **73**, 117 (2010).
[31] C. Raghu, I. Rudra, D. Sen, and S. Ramasesha, Phys. Rev. B **64**, 064419 (2001).
[32] C. Raghu, I. Rudra, D. Sen, and S. Ramasesha, Phys. Rev. B **68**, 029902 (2003).
[33] I. Rudra, S. Ramasesha, and D. Sen, Phys. Rev. B **64**, 014408 (2001).
[34] O. Waldmann, Phys. Rev. B **61**, 6138 (2000).
[35] C. Delfs, D. Gatteschi, L. Pardi, R. Sessoli, K. Wieghardt, and D. Hanke, Inorg. Chem. **32**, 3099 (1993).
[36] I. G. Bostrem, A. S. Ovchinnikov, and V. E. Sinitsyn, Theor. Math. Phys. **149**, 1527 (2006).
[37] V. E. Sinitsyn, I. G. Bostrem, and A. S. Ovchinnikov, J. Phys. A – Math. Theor. **40**, 645 (2007).
[38] R. Schnalle, Ph.D. thesis, Osnabrück University (2009).
[39] R. Schnalle and J. Schnack, Phys. Rev. B **79**, 104419 (2009).
[40] J. Schnack and R. Schnalle, Polyhedron **28**, 1620 (2009).
[41] V. Fack, S. N. Pitre, and J. van der Jeugt, Comp. Phys. Comm. **101**, 155 (1997).
[42] V. Fack, S. N. Pitre, and J. van der Jeugt, Comp. Phys. Comm. **86**, 105 (1995).
[43] R. Schnalle, A. Läuchli, and J. Schnack, Condens. Matter Phys. **12**, 331 (2009).
[44] J. Schnack, Dalton Trans. (2010), published online: http://dx.doi.org/10.1039/B925358K.
[45] J. Borras-Almenar, J. Clemente, E. Coronado, A. Palii, B. Tsukerblat, and R. Georges, J. Chem. Phys. **105**, 6892 (1996).
[46] J. M. Clemente-Juan, J. J. Borra's-Almenar, E. Coronado, A. V. Palii, and B. S. Tsukerblat, Inorg. Chem. **48**, 4557 (2009).
[47] J. J. Borrás-Almenar, S. Cardona-Serra, J. M. Clemente-Juan, E. Coronado, A. V. Palii, and B. Tsukerblat, J. Comp. Chem. (2010), published online; DOI: 10.1002/jcc.21400.
[48] D. Gatteschi, Adv. Mater. **6**, 635 (1994).
[49] E. Coronado, P. Delhaes, D. Gatteschi, and J. Miller, eds., *Localized and Itinerant Molecular Magnetism: From Molecular Assemblies to the Devices*, vol. 321 of *NATO Advanced Studies Institute, Series E: Applied Sciences* (Kluwer Academic, Dordrecht, 1996).
[50] S. J. Blundell and F. L. Pratt, J. Phys.: Cond. Mat. **16**, R771 (2004).
[51] S. J. Blundell, Contemp. Phys. **48**, 275 (2007).
[52] P. W. Anderson, Phys. Rev. **115**, 2 (1959).
[53] J. van Slageren, R. Sessoli, D. Gatteschi, A. Smith, M. Helliwell, R. Winpenny, A. Cornia, A. Barra, A. Jansen, E. Rentschler, and G. A. Timco, Chem. Eur. J. **8**, 277 (2002).
[54] S. Carretta, J. van Slageren, T. Guidi, E. Liviotti, C. Mondelli, D. Rovai, A. Cornia, A. L. Dearden, F. Carsughi, M. Affronte, C. Frost, R. Winpenny, D. Gatteschi, G. Amoretti, and R. Caciuffo, Phys. Rev. B **67**, 094405 (2003).
[55] M. Affronte, T. Guidi, R. Caciuffo, S. Carretta, G. Amoretti, J. Hinderer, I. Sheikin, A. G. M. Jansen, A. A. Smith, R. E. P. Winpenny, J. van Slageren, and D. Gatteschi, Phys. Rev. B **68**, 104403 (2003).
[56] B. L. Silver, *Irreducible Tensor Methods* (Academic Press, New York, 1976).
[57] E. P. Wigner, *Group Theory and Its Application to the Quantum Mechanics of Atomic Spectra* (Academic Press, New York, 1959).
[58] U. Fano and G. Racah, *Irreducible Tensor Sets* (Academic Press, New York, 1959).

[59] A. R. Edmonds, *Angular Momentum in Quantum Mechanics* (Princeton University Press, Princeton, 1957).
[60] E. U. Condon and G. H. Shortley, *The Theory of Atomic Spectra* (Cambridge University Press, New York, 1951).
[61] M. Tinkham, *Group Theory and Quantum Mechanics* (Dover Publications, New York, 2003).
[62] D. A. Varshalovich, A. N. Moskalev, and V. K. Khersonskii, *Quantum Theory of Angular Momentum* (World Scientific, Singapore, 1988).
[63] H. Lueken, *Magnetochemie*, Teubner Studienbücher Chemie (B.G. Teubner Stuttgart, Leipzig, 1999).
[64] A. J. Blake, R. O. Gould, C. M. Grant, P. E. Y. Milne, S. Parsons, and R. E. P. Winpenny, J. Chem. Soc. Dalton Trans. 485 (1997).
[65] A. Müller, S. Sarkar, S. Q. N. Shah, H. Bögge, M. Schmidtmann, S. Sarkar, P. Kögerler, B. Hauptfleisch, A. Trautwein, and V. Schünemann, Angew. Chem. Int. Ed. **38**, 3238 (1999).
[66] P. Kögerler, B. Tsukerblat, and A. Müller, Dalton Trans. **39**, 1 (2010).
[67] A. Müller, Science **300**, 749 (2003).
[68] T. Glaser, M. Heidemeier, E. Krickemeyer, H. Bögge, A. Stammler, R. Fröhlich, E. Bill, and J. Schnack, Inorg. Chem. **48**, 607 (2009).
[69] J. Schnack, Condens. Matter Phys. **12**, 323 (2009).
[70] I. S. Tidmarsh, L. J. Batchelor, E. Scales, R. H. Laye, L. Sorace, A. Caneschi, J. Schnack, and E. J. L. McInnes, Dalton Trans. 9402 (2009).
[71] G. S. Griffith, Structure and Bonding **10**, 87 (1972).
[72] F. A. Cotton, *Chemical Applications of Group Theory*, 3rd ed (John Wiley, New York, 1990).
[73] G. Racah, Phys. Rev. **62**, 438 (1942).
[74] K. L. Taft, C. D. Delfs, G. C. Papaefthymiou, S. Foner, D. Gatteschi, and S. J. Lippard, J. Am. Chem. Soc. **116**, 823 (1994).
[75] R. Schmidt, J. Schnack, and J. Richter, J. Magn. Magn. Mater. **295**, 164 (2005).
[76] C. Schröder, H.-J. Schmidt, J. Schnack, and M. Luban, Phys. Rev. Lett. **94**, 207203 (2005).
[77] J. Schnack, R. Schmidt, and J. Richter, Phys. Rev. B **76**, 054413 (2007).
[78] A. W. Sandvik and J. Kurkijärvi, Phys. Rev. B **43**, 5950 (1991).
[79] A. W. Sandvik, Phys. Rev. B **59**, R14157 (1999).
[80] L. Engelhardt and M. Luban, Phys. Rev. B **73**, 054430 (2006).
[81] A. Honecker and M. E. Zhitomirsky, J. Phys.: Conf. Ser. **145**, 012082 (4pp) (2009).
[82] M. Exler and J. Schnack, Phys. Rev. B **67**, 094440 (2003).
[83] U. Schollwöck, Rev. Mod. Phys. **77**, 259 (2005).
[84] E. Jeckelmann, Phys. Rev. B **66**, 045114 (2002).
[85] C. Lanczos, J. Res. Nat. Bur. Stand. **45**, 255 (1950).
[86] A. P. Ramirez, Annu. Rev. Mater. Sci. **24**, 453 (1994).
[87] J. Greedan, J. Mater. Chem. **11**, 37 (2001).
[88] H. Diep, ed., *Magnetic Systems with Competing Interactions* (World Scientific, Singapore, 1994).
[89] Y. Narumi, K. Katsumata, Z. Honda, J.-C. Domenge, P. Sindzingre, C. Lhuillier, Y. Shimaoka, T. C. Kobayashi, and K. Kindo, Europhys. Lett. **65**, 705 (2004).
[90] M. E. Zhitomirsky, Phys. Rev. Lett. **88**, 057204 (2002).
[91] J. Schulenburg, A. Honecker, J. Schnack, J. Richter, and H.-J. Schmidt, Phys. Rev. Lett. **88**, 167207 (2002).
[92] J. L. Atwood, Nat. Mater. **1**, 91 (2002).
[93] A. Müller, A. M. Todea, J. van Slageren, M. Dressel, H. Bögge, M. Schmidtmann, M. Luban, L. Engelhardt, and M. Rusu, Angew. Chem., Int. Ed. **44**, 3857 (2005).
[94] A. M. Todea, A. Merca, H. Bögge, J. van Slageren, M. Dressel, L. Engelhardt, M. Luban, T. Glaser, M. Henry, and A. Mäller, Angew. Chem. Int. Ed. **46**, 6106 (2007).
[95] C. P. Pradeep, D.-L. Long, P. Kögerler, and L. Cronin, Chem. Commun. 4254 (2007).

[96] J. Schnack, H.-J. Schmidt, J. Richter, and J. Schulenburg, Eur. Phys. J. B **24**, 475 (2001).
[97] C. Schröder, H. Nojiri, J. Schnack, P. Hage, M. Luban, and P. Kögerler, Phys. Rev. Lett. **94**, 017205 (2005).
[98] H.-J. Schmidt, J. Schnack, and M. Luban, Europhys. Lett. **55**, 105 (2001).
[99] O. Waldmann, Europhys. Lett. **57**, 618 (2002).
[100] H.-J. Schmidt, J. Schnack, and M. Luban, Europhys. Lett. **57**, 620 (2002).
[101] D. Coffey and S. A. Trugman, Phys. Rev. Lett. **69**, 176 (1992).
[102] N. P. Konstantinidis, Phys. Rev. B **72**, 064453 (2005).
[103] N. P. Konstantinidis, Phys. Rev. B **76**, 104434 (2007).
[104] E. I. Tolis, L. P. Engelhardt, P. V. Mason, G. Rajaraman, K. Kindo, M. Luban, A. Matsuo, H. Nojiri, J. Raftery, C. Schröder, G.A. Timco, F. Tuna, W. Wemsdorfer, and R.E.P. Winpenny, Chem. Eur. J. **12**, 8961 (2006).
[105] D. Gatteschi, A. Caneschi, L. Pardi, and R. Sessoli, Science **265**, 1054 (1994).
[106] A. Caneschi, A. Cornia, A. C. Fabretti, S. Foner, D. Gatteschi, R. Grandi, and L. Schenetti, Chem. Eur. J. **2**, 1379 (1996).
[107] R. Saalfrank, I. Bernt, E. Uller, and F. Hampel, Angew. Chem.-Int. Edit. Engl. **36**, 2482 (1997).
[108] G. Abbati, A. Caneschi, A. Cornia, A. Fabretti, and D. Gatteschi, Inorg. Chim. Acta **297**, 291 (2000).
[109] P. Santini, S. Carretta, G. Amoretti, T. Guidi, R. Caciuffo, A. Caneschi, D. Rovai, Y. Qiu, and J. R. D. Copley, Phys. Rev. B **71**, 184405 (2005).
[110] M.-H. Julien, Z. Jang, A. Lascialfari, F. Borsa, M. Horvatić, A. Caneschi, and D. Gatteschi, Phys. Rev. Lett. **83**, 227 (1999).
[111] J. Schnack and M. Luban, Phys. Rev. B **63**, 014418 (2000).
[112] O. Waldmann, Phys. Rev. B **65**, 024424 (2001).
[113] O. Waldmann, Phys. Rev. B **75**, 012415 (2007).
[114] O. Waldmann, T. C. Stamatatos, G. Christou, H. U. Güdel, I. Sheikin, and H. Mutka, Phys. Rev. Lett. **102**, 157202 (2009).
[115] A. P. Yutsis, I. B. Levinson, and V. V. Vanagas, *The Mathematical Aparatus of the Theory of Angular Momentum* (Israel Program for Scientific Translation, Jerusalem, 1962).
[116] P. G. Burke, Comp. Phys. Comm. **1**, 241 (1970).
[117] V. Fack, S. N. Pitre, and J. van der Jeugt, Comp. Phys. Comm. **83**, 275 (1994).
[118] B. Erbe and H. J. Schmidt, J. Phys. A – Math. Theor. **43**, 085215 (2010).
[119] A. Bar-Shalom and M. Klapisch, Comp. Phys. Comm. **50**, 375 (1988).
[120] P. M. Lima, Comp. Phys. Comm. **66**, 89 (1991).
[121] D. Van Dyck and V. Fack, Comp. Phys. Comm. **154**, 219 (2003).
[122] L. C. Biedenharn and J. D. Louck, *The Racah–Wigner Algebra in Quantum Theory*, Vol. 9 of *Encyclopedia of Mathematics and its Applications* (Addison-Wesley, Reading, MA, USA, 1981), p. 435.

A. Realization of the irreducible tensor operator technique

In this section the theoretical foundations presented in Section 2 shall be specified. To this end, after having developed a basic idea of the coupling of angular momenta a spin square deals as a small example system. It is demonstrated how an appropriate basis can be constructed and what the Heisenberg Hamiltonian looks like when expressed in terms of irreducible tensor operators. Later on, it is shown how the matrix elements can be evaluated by decoupling the irreducible tensor operator that describes the system. A central aspect is the use of point-group symmetries in combination with irreducible tensor operators that leads to the occurrence of general recoupling coefficients.

A.1. *Coupling of angular momenta and Wigner-nJ symbols*

As a first step the coupling of two general angular momenta $\mathbf{j}_1$ and $\mathbf{j}_2$ shall be discussed. Regarding this, the work at hand mainly refers to the use of definitions and name conventions that have been introduced by Wigner [57].

The vector coupling rule for the addition of angular momenta, known from elementary atomic physics, states that the resulting angular momenta $\mathbf{J}$ can be characterized by a quantum number J. J assumes all values

$$|j_1 - j_2|, |j_1 - j_2| + 1, \ldots, j_1 + j_2 - 1, j_1 + j_2, \tag{31}$$

where j_1 and j_2 denote the quantum numbers of the angular momenta $\mathbf{j}_1$ and $\mathbf{j}_2$. Equation (31) is also referred to as the triangular condition for the coupling of two angular momenta.

From a group-theoretical point of view the eigenstates $|jm\rangle$ of j^z and $\mathbf{j}^2$ span a $(2j+1)$-dimensional irreducible representation $D^{(j)}$ of the group R_3, i.e. the group of all rotations within three-dimensional space. Keeping this in mind, the above vector addition rule (31) is equivalent to

$$D^{(j_1)} \otimes D^{(j_2)} = \sum_{J=|j_1-j_2|}^{j_1+j_2} D^{(J)}. \tag{32}$$

According to this equation, the direct product between two irreducible representations of dimensions $(2j_1+1)$ and $(2j_2+1)$, which is in general reducible, decays into $(2J+1)$-dimensional irreducible representations with respect to J.

Now, the operators $D^{(j_1)}(R)$ and $D^{(j_2)}(R)$ are associated with an arbitrary coordinate rotation R of R_3 and operate in the Hilbert spaces spanned by $|j_1 m_1\rangle$ and $|j_2 m_2\rangle$. What does Equation (32) mean for the direct product $\mathbf{D}^{(j_1)}(R) \otimes \mathbf{D}^{(j_2)}(R)$ of the corresponding matrix representations? The product can be transformed into a block-diagonal form $\mathbf{U}(R)$ by a unitary matrix $\mathbf{A}$, i.e.

$$\mathbf{D}^{(j_1)}(R) \otimes \mathbf{D}^{(j_2)}(R) = \mathbf{A}^\dagger \mathbf{U}(R) \mathbf{A}, \tag{33}$$

where $\mathbf{U}(R)$ has the form

$$\mathbf{U}(R) = \begin{bmatrix} \mathbf{D}^{(|j_1-j_2|)}(R) & \mathbf{0} & \ldots & \mathbf{0} \\ \mathbf{0} & \mathbf{D}^{(|j_1-j_2|+1)}(R) & \ldots & \mathbf{0} \\ \vdots & \vdots & \ldots & \vdots \\ \mathbf{0} & \mathbf{0} & \ldots & \mathbf{D}^{(j_1+j_2)}(R) \end{bmatrix}.$$

The matrices $\mathbf{D}^{(J)}(R)$ appearing therein comprise matrix elements with respect to those functions that span the irreducible representations $D^{(J)}$ in Equation (32).

The determination of the elements of the transformation matrix $\mathbf{A}$ has been a central task in the theory of group representations. The elements of $\mathbf{A}$ are the so-called *Clebsch–Gordan coefficients* $C^{j_1 j_2 J}_{m_1 m_2 M}$. They appear in a more familiar form as scalar products between a state of the form $|j_1 j_2 J M\rangle$ and the product states $|j_1 m_1 j_2 m_2\rangle$ leading to the decomposition

$$\begin{aligned} |j_1 j_2 J M\rangle &= \sum_{m_1, m_2} \langle j_1 m_1 j_2 m_2 | j_1 j_2 J M \rangle | j_1 m_1 j_2 m_2 \rangle \\ &= \sum_{m_1, m_2} C^{j_1 j_2 J}_{m_1 m_2 M} | j_1 m_1 j_2 m_2 \rangle. \end{aligned} \tag{34}$$

The Clebsch–Gordan coefficients therefore relate two different orthonormal sets of basis vectors. It should be emphasized that these sets are obviously not orthogonal to each other because they span the same space. The Clebsch–Gordan coefficients are non-zero only if the vector addition rule from Equation (31) and simultaneously the equation $m_1 + m_2 = M$ hold. A very important symmetry of the Clebsch–Gordan coefficients is

$$C^{j_1 j_2 J}_{m_1 m_2 M} = (-1)^{j_1 + j_2 - J} C^{j_2 j_1 J}_{m_2 m_1 M}, \tag{35}$$

with $(-1)^{j_1+j_2-J} = \pm 1$ according to Equation (31).

In order to reveal the symmetry properties of the Clebsch–Gordan coefficients, they are reformulated in a straightforward manner. A proper reformulation leads to the *Wigner coefficients* or *Wigner-3J symbols*

$$\begin{pmatrix} j_1 & j_2 & J \\ m_1 & m_2 & M \end{pmatrix},$$

which are related to the Clebsch–Gordan coefficients by

$$\begin{pmatrix} j_1 & j_2 & J \\ m_1 & m_2 & M \end{pmatrix} = (-1)^{j_1-j_2-M}(2J+1)^{-\frac{1}{2}} C^{j_1 j_2 J}_{m_1 m_2 -M}. \tag{36}$$

The relation between Clebsch–Gordan coefficients and the Wigner-3J symbols from Equation (36) directly leads to non-zero values of the Wigner-3J symbols only if $m_1 + m_2 + M = 0$ holds and the vector addition rule from Equation (31) is fulfilled.

Expressed in terms of Wigner-3J symbols the symmetry property of the Clebsch–Gordan coefficients given in Equation (35) takes the form

$$\begin{pmatrix} j_1 & j_2 & J \\ m_1 & m_2 & M \end{pmatrix} = (-1)^{j_1+j_2+J} \begin{pmatrix} j_2 & j_1 & J \\ m_2 & m_1 & M \end{pmatrix}. \tag{37}$$

Thus, the Wigner-3J symbols are invariant under an even number of permutations of the columns whereas under a single permutation they obey Equation (37). A further evaluation of the symmetry properties of the Clebsch–Gordan coefficients yields an additional symmetry of the Wigner-3J symbols, i.e.

$$\begin{pmatrix} j_1 & j_2 & J \\ m_1 & m_2 & M \end{pmatrix} = (-1)^{j_1+j_2+J} \begin{pmatrix} j_1 & j_2 & J \\ -m_1 & -m_2 & -M \end{pmatrix}. \tag{38}$$

So far the coupling of only two angular momenta has been considered. A procedure similar to the one which has led to the Wigner-3J symbols now leads to the occurrence of *Wigner-6J symbols*. In the case of a coupling of three angular momenta, $\underset{\sim}{\mathbf{J}} = \underset{\sim}{\mathbf{j}}_1 + \underset{\sim}{\mathbf{j}}_2 + \underset{\sim}{\mathbf{j}}_3$, a basis can be constructed in which the representations of the operators $\underset{\sim}{\mathbf{J}}^2$ and $\underset{\sim}{J}^z$ as well as $\underset{\sim}{\mathbf{j}}_1^2, \underset{\sim}{\mathbf{j}}_2^2$, and $\underset{\sim}{\mathbf{j}}_3^2$ are diagonal. Obviously, there exists a certain freedom of choice in the construction of this basis. The resulting $\underset{\sim}{\mathbf{J}}$ can be constructed in three different ways, namely

$$\underset{\sim}{\mathbf{J}} = (\underset{\sim}{\mathbf{j}}_1 + \underset{\sim}{\mathbf{j}}_2) + \underset{\sim}{\mathbf{j}}_3, \tag{39}$$

$$\underset{\sim}{\mathbf{J}} = \underset{\sim}{\mathbf{j}}_1 + (\underset{\sim}{\mathbf{j}}_2 + \underset{\sim}{\mathbf{j}}_3), \tag{40}$$

$$\underset{\sim}{\mathbf{J}} = (\underset{\sim}{\mathbf{j}}_1 + \underset{\sim}{\mathbf{j}}_3) + \underset{\sim}{\mathbf{j}}_2. \tag{41}$$

This leads to three different basis sets, each with the square of one of the operators $\underset{\sim}{\mathbf{j}}' = \underset{\sim}{\mathbf{j}}_1 + \underset{\sim}{\mathbf{j}}_2$, $\underset{\sim}{\mathbf{j}}'' = \underset{\sim}{\mathbf{j}}_2 + \underset{\sim}{\mathbf{j}}_3$, and $\underset{\sim}{\mathbf{j}}''' = \underset{\sim}{\mathbf{j}}_1 + \underset{\sim}{\mathbf{j}}_3$ given in diagonal form. The matrix elements of the unitary transformation matrix which connects two of these sets of basis states can be found as scalar products between states belonging to two different *coupling schemes*. Expressing a state belonging to a coupling scheme resulting from a coupling according to Equation (39) in terms of states belonging to the scheme resulting from Equation (40) yields

$$|j_1 j_2 j_{12} j_3 J M\rangle = \sum_{j_{23}} \langle j_1 j_2 j_3 j_{23} J | j_1 j_2 j_{12} j_3 J\rangle |j_1 j_2 j_3 j_{23} J M\rangle, \tag{42}$$

with the quantum numbers j_{12} and j_{23} referring to $\mathbf{j}'^2$ and $\mathbf{j}''^2$, respectively.

Scalar products of the kind found in Equation (42) – often called *recoupling coefficients* – are independent of any magnetic quantum number. They can be evaluated by decomposing

the vector-coupling states into a sum of product states with the help of an extended version of Equation (34). For example, the decomposition of the ket on the left-hand side of the aforementioned recoupling coefficients yields

$$|j_1 j_2 j_3 j_{23} JM\rangle = \sum_{m_1,m_2,m_3} \langle j_1 m_1 j_2 m_2 j_3 m_3 | j_1 j_2 j_3 j_{23} JM\rangle \times |j_1 m_1 j_2 m_2 j_3 m_3\rangle. \tag{43}$$

The scalar products in Equation (43), i.e. the matrix elements of the transformation matrix that connects the vector-coupling state with the product states, are called in analogy to the former name convention *generalized Clebsch–Gordan coefficients* $C^{j_1 j_2 j_3 j_{23} J}_{m_1 m_2 m_3 m_{23} M}$ for the coupling of three angular momenta. They can be simplified to a product of Clebsch–Gordan coefficients according to

$$C^{j_1 j_2 j_3 j_{23} J}_{m_1 m_2 m_3 m_{23} M} = \sum_{m_{23}} C^{j_2 j_3 j_{23}}_{m_2 m_3 m_{23}} \cdot C^{j_1 j_{23} J}_{m_1 m_{23} M}. \tag{44}$$

As one can see, generating generalized Clebsch–Gordan coefficients for the coupling of more than three angular momenta and – in addition – an expression of it in terms of Clebsch–Gordan coefficients is then a straightforward task. Here it should be mentioned that according to Equation (44) generalized Clebsch–Gordan coefficients can also be expressed as a sum over products of Wigner-3J symbols using the relation from Equation (36). Coefficients of this kind are then called *generalized Wigner coefficients* [115].

The recoupling coefficients that appear in Equation (42) can now be reformulated in terms of Wigner-6J symbols in order to reveal their symmetry properties. For the transition between the basis sets belonging to j_{12} and j_{23} the corresponding Wigner-6J symbol is related to the recoupling coefficient by [57]

$$\begin{Bmatrix} j_1 & j_2 & j_{12} \\ j_3 & J & j_{23} \end{Bmatrix} = (-1)^{j_1+j_2+j_3+J}(2j_{12}+1)^{-\frac{1}{2}} \times (2j_{23}+1)^{-\frac{1}{2}} \langle j_1 j_2 j_3 j_{23} J | j_1 j_2 j_{12} j_3 J\rangle. \tag{45}$$

Equations (43) and (44) directly show that a Wigner-6J symbol can be expressed as a sum over products of Clebsch–Gordan coefficients or, by using Equation (36), over products of Wigner-3J symbols.

For the sake of completeness, also the Wigner-9J symbols [57] shall be given which result as elements of the transition matrices when recoupling four angular momenta. For example the transition between two different sets of basis states yields a Wigner-9J symbol like

$$\begin{pmatrix} j_1 & j_2 & j_{12} \\ j_3 & j_4 & j_{34} \\ j_{13} & j_{24} & J \end{pmatrix} = [(2j_{12}+1)(2j_{34}+1)(2j_{13}+1)(2j_{24}+1)]^{-\frac{1}{2}} \times \langle j_1 j_2 j_{12} j_3 j_4 j_{34} J | j_1 j_3 j_{13} j_2 j_4 j_{24} J\rangle. \tag{46}$$

A very comprehensive overview of algebraic expressions for Wigner-nJ symbols as well of their symmetry properties is given in Ref. [62]. Regarding the use of Wigner symbols in connection with irreducible tensor operators, here only a graphical visualization of the triangular conditions for a Wigner-6J symbol is shown. The Wigner-6J symbol is non-zero only if for certain triads of quantum numbers the triangular condition (Equation (31)) holds. For which combination of quantum numbers of angular momenta the triangular condition has to be valid in order to yield a non-zero Wigner-6J symbol, is visualized graphically in Figure 14.

Since a Wigner-9J symbol can be written as a sum over products of Wigner-6J symbols [62], these triangular conditions play an important role in reducing the computational effort when matrix elements of the Heisenberg Hamiltonian are calculated using irreducible tensor operators.

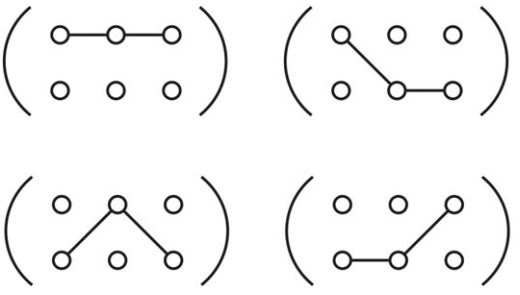

Figure 14. Graphical visualization of the four triangular conditions occurring in a Wigner-6J symbol which have to be valid in order to yield a non-zero result.

A.2. *The construction of basis states*

The reduction of the dimensionalities of the Hilbert spaces in which the Hamilton matrices are set up in order to solve the eigenvalue problem is always a desirable, but also numerically involved task. Especially if the basis a priori reflects symmetry properties of the system, an appropriate choice can be of great help. As mentioned in Section 2, a basis that consists of vector-coupling states and incorporates full spin-rotational ($SU(2)$) symmetry would be the first choice. In isotropic spin systems as described by a Heisenberg Hamiltonian the Hamilton matrix is then block-diagonalized with respect to S and M without further calculations since there are no transition elements between states of a different total magnetic quantum number M and different total-spin quantum number S.

The vector-coupling states used in the present work appear in the form $|\alpha SM\rangle$. α denotes a set of intermediate quantum numbers resulting from the chosen coupling scheme according to which the spins are coupled. As mentioned in the previous section the choice of the coupling scheme is somewhat arbitrary since it only reflects the bracketing in the expression for the total spin operator of the system $\underset{\sim}{\mathbf{S}} = \sum_i \underset{\sim}{\mathbf{s}}_i$.

The simplest choice of a coupling scheme would probably be a successive coupling of the single-spin vector operators $\underset{\sim}{\mathbf{s}}_i$. In the case of a spin square the set of intermediate quantum numbers, if coupled according to a successive coupling scheme, looks like

$$\alpha = \{s_{12} = \overline{S}_1, s_{123} = \overline{S}_2\}$$

leading to a vector-coupling state of the form $|s_1 s_2 \overline{S}_1 s_3 \overline{S}_2 s_4 SM\rangle$. Here, the notation of the intermediate spin quantum numbers, i.e. s_{12} and s_{123}, is changed in comparison to Appendix A.1. Intermediate spins are now numbered with respect to their order of appearance in the coupling scheme and additionally overlined. This notation has a clear advantage if larger spin systems are investigated and is used in the following. In order to clarify which spins are coupled, the single-spin quantum numbers s_i can also be found in the ket. It would not be necessary to include them since they appear as fixed numbers, but it turns out to be more convenient.

Now, if the coupling scheme is chosen and the framework of the resulting basis states is fixed, one has to construct the basis states by finding those values of the intermediate spins that are valid according to Equation (31). This procedure can be visualized by constructing a coupling pyramid as shown in Figure 15. In Figure 15 four spins with $s = 1$ are successively coupled in order to yield the values of the total-spin quantum number S. The (red) subscripts next to the quantum numbers of the intermediate spins denote the number of different paths leading to the same value for an intermediate spin quantum number, i.e. the multiplicity. The small (gray) numbers interrupting the lines connecting different intermediate spin quantum numbers indicate the quantum numbers of the single spins, i.e. $s_i = 1$. For the sake of clarity, on the left of Figure 15 the underlying coupling scheme is given once more.

Of course, a successive coupling scheme is not the only possible way to couple the single spins $\underset{\sim}{\mathbf{s}}_i$ to a total spin $\underset{\sim}{\mathbf{S}}$. For example, the construction of quasi-classical states as described in Refs. [39] and

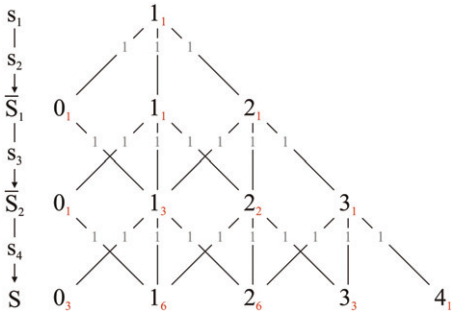

Figure 15. [Colour online] Successive coupling of four spins $s=1$. The (red) subscripts denote the multiplicity, i.e. the number of paths leading to the spin quantum number. The gray numbers refer to the spin quantum numbers of the coupled single spins. On the left the coupling scheme is indicated.

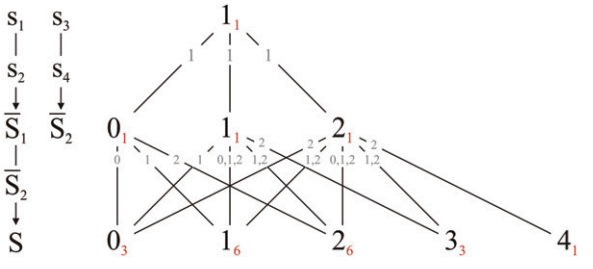

Figure 16. [Colour online] Pairwise coupling of four spins $s=1$. The (red) subscripts denote the multiplicity, i.e. the number of paths leading to the spin quantum number. The gray numbers refer to the spin quantum numbers of the coupled single or intermediate spins. On the left the coupling scheme is indicated.

[40] requires a different coupling scheme. There, a coupling scheme is chosen in which spins belonging to a certain sublattice are coupled in order to get the total sublattice spin that is afterwards coupled to the total spin of the system. In Figure 16 a coupling pyramid for a different coupling scheme of a spin square is shown. The spins $\underset{\sim}{\mathbf{s}}_1$, $\underset{\sim}{\mathbf{s}}_2$ and $\underset{\sim}{\mathbf{s}}_3$, $\underset{\sim}{\mathbf{s}}_4$ are coupled to yield intermediate spins $\underset{\sim}{\overline{\mathbf{S}}}_1$ and $\underset{\sim}{\overline{\mathbf{S}}}_2$, respectively. The intermediate spins are then coupled to the total spin $\underset{\sim}{\mathbf{S}}$.

The resulting multiplicity of states with the same quantum number S is obviously independent of the chosen coupling scheme. At this point it is important to realize once again that these states, although resulting from different coupling schemes, form basis sets of the same Hilbert space $\mathcal{H}$. In the case of a square the coupling of four single spins $s=1$ discussed above results in basis states that span the subspaces $\mathcal{H}(S)$ with $S=0,1,\ldots,4$. Writing this result in a different way using Equation (22), one obtains for the direct product of the irreducible representations $D^{(1)}$ of the single spins the following expression:

$$D^{(1)} \otimes D^{(1)} \otimes D^{(1)} \otimes D^{(1)} = 3 \cdot D^{(0)} + 6 \cdot D^{(1)} + 6 \cdot D^{(2)} + 3 \cdot D^{(3)} + 1 \cdot D^{(4)}.$$

Knowledge of the dimensions of the resulting irreducible representations, i.e. subspaces $\mathcal{H}(S)$, is a central task whenever performing numerical exact diagonalization. Deduced from a successive coupling of the spins, the dimensions dim $\mathcal{H}(S)$ can be calculated by a simple recurrence formula.

The number of paths leading to a certain combination (S,n) is denoted by d_S. n refers to the number of participating spins in each step and runs from 1 to N. n can also be seen as labeling the

rows of the coupling pyramid for a successive coupling (see Figure 15). In the case of a homonuclear system with N spins s, the multiplicity $d_S(S, n+1)$ is given by

$$d_S(S, n+1) = \sum_{S'=|S-s|}^{\min(S+s,\, n\cdot s)} d_S(S', n), \tag{47}$$

where S lies in the interval that is bounded by

$$(n+1)s \geq S \geq \begin{cases} 0 & \text{if } 2s(n+1) \text{ even} \\ \frac{1}{2} & \text{if } 2s(n+1) \text{ odd} \end{cases} \tag{48}$$

according to a vector coupling rule (cf. Equation (31)). The number of paths leading to a certain quantum number S for one spin is just

$$d_S(S, 1) = \begin{cases} 1 & \text{if } S = s \\ 0 & \text{else.} \end{cases} \tag{49}$$

The dimension of the Hilbert space $\mathcal{H}(S)$ is then given by dim $\mathcal{H}(S) = d_S(S, N) \cdot (2S+1)$.

The dimensions within a heteronuclear spin system, i.e. a system with different values of single-spin quantum numbers, are obtained along the same route. However, the range of valid values for S has to be calculated for each step of recurrence separately, in contrast to the use of Equation (48). Furthermore, the sum in Equation (47) would run from $S' = |S - s_i|$ to $\min(S + s_i, \sum_{i=1}^{n} s_i)$ where the spin quantum number of every single spin s_i is individually labeled by the index i.

A.3. *The Heisenberg Hamiltonian expressed as an irreducible tensor operator*

In order to determine the spectra of magnetic molecules as it is done throughout this work, the Heisenberg Hamiltonian of Equation (30) has to be expressed as an irreducible tensor operator. In this section a general expression for the Heisenberg Hamiltonian is presented which can be used as a starting point for the calculation of the energy spectrum using the irreducible tensor operator approach.

Spin dimer – The first step in finding an expression for the Heisenberg Hamiltonian in the form of an irreducible tensor operator is done by considering a spin dimer. The Hamiltonian of the dimer takes the simple form

$$\underset{\sim}{H}_{\text{dimer}} = -J\, \underset{\sim}{\mathbf{s}}(1) \cdot \underset{\sim}{\mathbf{s}}(2). \tag{50}$$

Now, using Equation (13) the above Equation (50) can easily be reproduced. Since the Heisenberg term is given by a scalar product, the corresponding compound irreducible tensor operator is of rank $k = 0$. Using Equations (12)–(15) one finds the expression

$$\begin{aligned} \left\{ \underset{\sim}{\mathbf{s}}^{(1)}(1) \otimes \underset{\sim}{\mathbf{s}}^{(1)}(2) \right\}^{(0)} &= \sum_{q_1, q_2} C^{1\,1\,0}_{q_1\, q_2\, 0} \cdot \underset{\sim}{s}^{(1)}_{q_1}(1) \underset{\sim}{s}^{(1)}_{q_2}(2) \\ &= \frac{1}{\sqrt{3}} \left(\underset{\sim}{s}^{(1)}_{-1}(1) \cdot \underset{\sim}{s}^{(1)}_{1}(2) + \underset{\sim}{s}^{(1)}_{1}(1) \cdot \underset{\sim}{s}^{(1)}_{-1}(2) - \underset{\sim}{s}^{(1)}_{0}(1) \cdot \underset{\sim}{s}^{(1)}_{0}(2) \right) \\ &= -\frac{1}{\sqrt{3}}\, \underset{\sim}{\mathbf{s}}(1) \cdot \underset{\sim}{\mathbf{s}}(2). \end{aligned}$$

Thus, the tensorial form of the Heisenberg Hamiltonian of a spin dimer is

$$\underset{\sim}{H}_{\text{dimer}} = \sqrt{3} J \left\{ \underset{\sim}{\mathbf{s}}^{(1)}(1) \otimes \underset{\sim}{\mathbf{s}}^{(1)}(2) \right\}^{(0)}. \tag{51}$$

Spin triangle – Since the tensorial form of $\underset{\sim}{H}_{\text{dimer}}$ in Equation (51) describes a simple bilinear spin–spin interaction, an expression for a general Heisenberg Hamiltonian can now be developed.

As a first extension a spin triangle is considered. The Hamiltonian that has to be converted to an irreducible tensor operator is

$$\underset{\sim}{H}_{\triangle} = -J\left(\underset{\sim}{\mathbf{s}}(1)\cdot\underset{\sim}{\mathbf{s}}(2)+\underset{\sim}{\mathbf{s}}(2)\cdot\underset{\sim}{\mathbf{s}}(3)+\underset{\sim}{\mathbf{s}}(3)\cdot\underset{\sim}{\mathbf{s}}(1)\right). \tag{52}$$

In a very general form the successive coupling of three single-spin irreducible tensor operators of ranks k_1, k_2 and k_3 leads to

$$\underset{\sim}{\mathbf{T}}^{(k)}_{\therefore}(k_1,k_2,k_3,\overline{k}_1) = \left\{\left\{\underset{\sim}{\mathbf{s}}^{(k_1)}(1)\otimes\underset{\sim}{\mathbf{s}}^{(k_2)}(2)\right\}^{(\overline{k}_1)}\otimes\underset{\sim}{\mathbf{s}}^{(k_3)}(3)\right\}^{(k)}. \tag{53}$$

Here k denotes the rank of the resulting irreducible tensor operator and $\overline{k}_1$ the rank of the intermediate (coupled) one. The ranks of the many-particle tensor operators are given by the coupling rules for spin quantum numbers known from the spin vector coupling. For example, the rank $\overline{k}_1$is given by $\overline{k}_1 = |k_1-k_2|, |k_1-k_2|+1,\ldots,k_1+k_2$ with k being determined accordingly. It must be emphasized that $\underset{\sim}{\mathbf{T}}^{(k)}_{\therefore}$ includes all spin–spin interactions of a trimeric spin system, and thus it has to be specified in order to give the desired tensorial formulation of $\underset{\sim}{H}_{\triangle}$. To indicate this difference we used the index $\therefore$ in $\underset{\sim}{\mathbf{T}}^{(k)}_{\therefore}$ and $\triangle$ in $\underset{\sim}{H}_{\triangle}$.

With $\underset{\sim}{\mathbf{s}}^{(0)} = \underset{\sim}{\mathbf{1}}$ and the tensorial expression found for a bilinear coupling in Equation (51) one arrives at

$$\begin{aligned}\underset{\sim}{H}_{\triangle} &= \sqrt{3}J\left(\underset{\sim}{T}^{(0)}_{\therefore}(1,1,0,0)+\underset{\sim}{T}^{(0)}_{\therefore}(1,0,1,1)+\underset{\sim}{T}^{(0)}_{\therefore}(0,1,1,1)\right)\\ &= \sqrt{3}J\sum_{\langle i,j\rangle}\underset{\sim}{T}^{(0)}_{\therefore}(\{k_i\},\{\overline{k}_i\}|k_i=k_j=1).\end{aligned} \tag{54}$$

The notation $\underset{\sim}{T}^{(0)}_{\therefore}(\{k_i\},\{\overline{k}_i\}|k_i=k_j=1)$ indicates that only the ranks of single-spin tensor operators i and j are chosen to equal 1 whereas the other tensor operators are of zero rank. The rank of the intermediate tensor operator $\overline{k}_1$ is fixed by the contributions of k_1 and k_2 to the zero-rank tensor operator $\underset{\sim}{\mathbf{T}}^{(k=0)}_{\therefore}$.

Following Equations (51) and (54), the Heisenberg Hamiltonian of a general spin system is given by

$$\underset{\sim}{H}_{\text{Heisenberg}} = \sqrt{3}\sum_{\langle i,j\rangle}J_{ij}\,\underset{\sim}{T}^{(0)}(\{k_i\},\{\overline{k}_i\}|k_i=k_j=1), \tag{55}$$

where the irreducible tensor operator $\underset{\sim}{\mathbf{T}}^{(k)}(\{k_i\},\{\overline{k}_i\})$ directly depends on the investigated system and the chosen coupling scheme for the coupling of the single-spin tensor operators $\underset{\sim}{\mathbf{s}}^{(k_i)}(i)$.

As an example, the resulting expression for the general, tetrameric tensor operator $\underset{\sim}{\mathbf{T}}^{(k)}_{\therefdots}$ in the case of a spin square shall be presented. The underlying coupling scheme of the single-spin tensor operators is chosen to be pairwise because it is often advantageous to couple this way when additionally point-group symmetries are used (see Appendix A.5). Then, the general irreducible tensor operator of a tetrameric system takes the form

$$\begin{aligned}\underset{\sim}{\mathbf{T}}^{(k)}_{\therefdots}(k_1,k_2,k_3,k_4,\overline{k}_1,\overline{k}_2) = \Big\{&\left\{\underset{\sim}{\mathbf{s}}^{(k_1)}(1)\otimes\underset{\sim}{\mathbf{s}}^{(k_2)}(2)\right\}^{(\overline{k}_1)}\\ &\otimes\left\{\underset{\sim}{\mathbf{s}}^{(k_3)}(3)\otimes\underset{\sim}{\mathbf{s}}^{(k_4)}(4)\right\}^{(\overline{k}_2)}\Big\}^{(k)}.\end{aligned} \tag{56}$$

Again, as for $\underset{\sim}{\mathbf{T}}^{(k)}_{\therefdots}$, Equation (53) also $\underset{\sim}{\mathbf{T}}^{(k)}_{\therefdots}$ includes all spin–spin interactions of a tetrameric spin system, and thus it has to be specified in order to give the tensorial formulation of the desired four-spin Hamiltonian.

The values of the ranks appearing in Equation (56) for the spin square modeled by a Heisenberg Hamiltonian are shown in Table 1. The ranks of the single-spin tensor operators are fixed by the particular spin–spin interaction. Then, the ranks of the intermediate tensor operators $\overline{k}_1$ and $\overline{k}_2$ can be constructed from the known coupling rules with the given ranks k_i, $i=1,\ldots,4$, so as to yield an irreducible tensor operator with $k=0$.

Table 1. Values of the ranks for a spin square described by a Heisenberg Hamiltonian. The rows refer to the nearest-neighbor interaction $\langle i,j\rangle$ between single spins i and j.

	k_1	k_2	k_3	k_4	$\overline{k}_1$	$\overline{k}_2$	k
$\langle 1,2\rangle$	1	1	0	0	0	0	0
$\langle 2,3\rangle$	0	1	1	0	1	1	0
$\langle 3,4\rangle$	0	0	1	1	0	0	0
$\langle 4,1\rangle$	1	0	0	1	1	1	0

A.4. *Matrix elements – decoupling*

The calculations of the matrix elements of the Hamiltonian in Equation (55) are performed with the help of the Wigner–Eckart theorem [12–17]. For this reason, the coupling scheme of the basis states $|\alpha SM\rangle$ cannot be chosen independently from $\underset{\sim}{\mathbf{T}}^{(k)}_{::}$. Those quantum numbers which appear within the set α should also appear in the sets $\{k_i\}$ and $\{\overline{k}_i\}$, i.e. the couplings for the generation of the basis states and the general irreducible tensor operator of the system should be chosen to be equal. Otherwise, transformations between states of different coupling schemes would be necessary.

In order to show how matrix elements can be calculated, the application of the *decoupling* procedure is discussed for a square system. The Heisenberg Hamiltonian in tensorial form can be derived from Equation (55) and is given by

$$\underset{\sim}{H}_{\square} = \sqrt{3}J \sum_{\langle i,j\rangle} \underset{\sim}{T}^{(0)}_{::}(\{k_i\},\{\overline{k}_i\}|k_i = k_j = 1). \tag{57}$$

The general irreducible tensor operator of the tetrameric system $\underset{\sim}{\mathbf{T}}^{(k)}_{::}$ based on a pairwise coupling scheme was already presented in Equation (56). The values of the ranks appearing in $\underset{\sim}{T}^{(k=0)}_{::}(\{k_i\},\{\overline{k}_i\})$ are tabulated in Table 1. The pairwise coupling scheme in the used construction of $\underset{\sim}{\mathbf{T}}^{(k)}_{::}$ corresponds to basis states of the form

$$|\alpha SM\rangle = |s_1 s_2 \overline{S}_1 s_3 s_4 \overline{S}_2 SM\rangle.$$

By the application of the Wigner–Eckart theorem the calculation of the matrix elements of $\underset{\sim}{H}_{\square}$ is now – apart from the prefactor and the summation over the nearest-neighbor interactions according to Equation (57) – reduced to the evaluation of terms like

$$\begin{aligned}\langle \alpha SM|\underset{\sim}{T}^{(0)}_{::}(\{k_i\},\{\overline{k}_i\})|\alpha' S' M'\rangle = (-1)^{S-M}&\begin{pmatrix} S & 0 & S' \\ -M & 0 & M' \end{pmatrix} \\ &\times \left\langle s_1 s_2 \overline{S}_1 s_3 s_4 \overline{S}_2 S \middle\| \underset{\sim}{\mathbf{T}}^{(0)}_{::} \middle\| s_1 s_2 \overline{S}'_1 s_3 s_4 \overline{S}'_2 S' \right\rangle. \end{aligned} \tag{58}$$

In the case of a square four such terms appear in $\underset{\sim}{H}_{\square}$ differing from each other by the values of $\{k_i\}$ and $\{\overline{k}_i\}$.

Since the Wigner-3J symbol in Equation (58) is reduced to

$$\begin{pmatrix} S & 0 & S' \\ -M & 0 & M' \end{pmatrix} = \frac{(-1)^{S-M}}{\sqrt{2S+1}} \cdot \delta_{S,S'}\delta_{M,M'}$$

Equation (58) itself is reduced to

$$\begin{aligned}\left\langle \alpha SM \middle| \underset{\sim}{T}^{(0)}_{::}(\{k_i\},\{\overline{k}_i\}) \middle| \alpha' S' M' \right\rangle &= \delta_{S,S'}\delta_{M,M'} \\ &\times \frac{(-1)^{2(S-M)}}{\sqrt{2S+1}} \cdot \left\langle s_1 s_2 \overline{S}_1 s_3 s_4 \overline{S}_2 S \middle\| \underset{\sim}{\mathbf{T}}^{(0)}_{::} \middle\| s_1 s_2 \overline{S}'_1 s_3 s_4 \overline{S}'_2 S \right\rangle. \end{aligned} \tag{59}$$

Since all matrix elements between states of different S and M vanish, it becomes obvious that all calculations can be performed in subspaces $\mathcal{H}(S, M)$. Furthermore, because $\underset{\sim}{H}_{\square}$ is independent of an external magnetic field and thus no M-dependence of the energies is given, the spectrum can be evaluated in subspaces $\mathcal{H}(S, M = S)$.

Following Equation (59) the matrix elements can directly be obtained by determining the reduced matrix elements of $\underset{\sim}{\underset{\cdot\cdot}{\mathbf{T}}}^{(0)}$. By a successive application of Equation (19), i.e. a successive decoupling of $\underset{\sim}{\underset{\cdot\cdot}{\mathbf{T}}}^{(0)}$, the reduced matrix elements are traced back to the reduced matrix elements of single-spin tensor operators that are given in Equations (17) and (18) for $k = 0, 1$.

For the reduced matrix element of $\underset{\sim}{\underset{\cdot\cdot}{\mathbf{T}}}^{(k)}$ the decoupling yields

$$\begin{aligned}
&\left\langle s_1 s_2 \overline{S}_1 s_3 s_4 \overline{S}_2 S \middle\| \underset{\sim}{\underset{\cdot\cdot}{\mathbf{T}}}^{(k)} \middle\| s_1 s_2 \overline{S}'_1 s_3 s_4 \overline{S}'_2 S' \right\rangle \\
&= \left[(2S+1)(2S'+1)(2k+1)\right]^{\frac{1}{2}} \left[(2\overline{S}_2+1)(2\overline{S}'_2+1)(2\overline{k}_2+1)\right]^{\frac{1}{2}} \left[(2\overline{S}_1+1)(2\overline{S}'_1+1)(2\overline{k}_1+1)\right]^{\frac{1}{2}} \\
&\quad \times \begin{pmatrix} \overline{S}_1 & \overline{S}'_1 & \overline{k}_1 \\ \overline{S}_2 & \overline{S}'_2 & \overline{k}_2 \\ S & S' & k \end{pmatrix} \begin{pmatrix} s_3 & s_3 & k_3 \\ s_4 & s_4 & k_4 \\ \overline{S}_2 & \overline{S}'_2 & \overline{k}_2 \end{pmatrix} \begin{pmatrix} s_1 & s_1 & k_1 \\ s_2 & s_2 & k_2 \\ \overline{S}_1 & \overline{S}'_1 & \overline{k}_1 \end{pmatrix} \\
&\quad \times \left\langle s_1 \middle\| \underset{\sim}{\mathbf{s}}^{(k_1)} \middle\| s_1 \right\rangle \left\langle s_2 \middle\| \underset{\sim}{\mathbf{s}}^{(k_2)} \middle\| s_2 \right\rangle \left\langle s_3 \middle\| \underset{\sim}{\mathbf{s}}^{(k_3)} \middle\| s_3 \right\rangle \left\langle s_4 \middle\| \underset{\sim}{\mathbf{s}}^{(k_4)} \middle\| s_4 \right\rangle . \qquad (60)
\end{aligned}$$

In the case of $\underset{\sim}{H}_{\square}$, the ranks of the tensor operators can be found in Table 1 and S' is forced to be $S' = S$ by the Wigner-3J symbol in Equation (58).

The clear structure of the resulting expression for a reduced matrix element in Equation (60) now allows one to write a highly flexible and structured computer program that takes over the calculation and diagonalization of the Hamilton matrix. Regarding the calculation of the matrix elements, a recurrence formula can be implemented which decouples the irreducible tensor operator of the system step-by-step [18].

A.5. *Using point-group symmetries*

General considerations concerning the use of point-group symmetries in Heisenberg spin systems have already been presented in Sections 2.3 and 2.4. Now, as a clarification of these considerations, a π-rotation around the central C_2-axis of a spin square is considered (cf. Figure 17). According to a successive coupling scheme, the vector-coupling basis states are given in the form $|s_1 s_2 \overline{S}_1 s_3 \overline{S}_2 s_4 S M\rangle$. It must be emphasized here that the underlying coupling scheme, which determines the way basis states are constructed, can be chosen independently of any symmetry considerations, although a suitable choice will reduce the calculations as discussed below.

Figure 17 shows the coupling graph of the square with D_4-symmetry operations. The operations are labeled with respect to n-fold rotations around the given axes. Operations belonging to the same

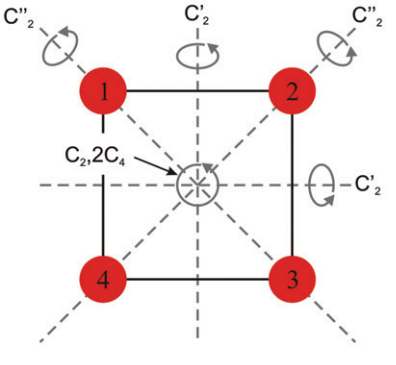

Figure 17. [Colour online] Sketch of a spin square with D_4-symmetry operations.

class are marked with identical labels while identical operations belonging to different classes can be distinguished by the number of primes.

In Table 2 the operators corresponding to the D_4-symmetry operations on the square are given. The operators are classified with respect to the classes they belong to. The mentioned operator that acts in spin space and corresponds to a π-rotation around the central axis takes the form $\underset{\sim}{G}(3\,4\,1\,2)$.

According to the generalized Clebsch–Gordan coefficients for the coupling of four spins and Equation (44), unfolding the state $|s_1 s_2 \overline{S}_1 s_3 \overline{S}_2 s_4 SM\rangle$ into a linear combination of product states results in the expression

$$|s_1 s_2 \overline{S}_1 s_3 \overline{S}_2 s_4 SM\rangle = \sum_{\sum_i m_i = M} C^{s_1 s_2 \overline{S}_1}_{m_1 m_2 \overline{M}_1} \cdot C^{\overline{S}_1 s_3 \overline{S}_2}_{\overline{M}_1 m_3 \overline{M}_2} \cdot C^{\overline{S}_2 s_4 S}_{\overline{M}_2 m_4 M} \times |m_1 m_2 m_3 m_4\rangle. \tag{61}$$

The summation indices are entirely determined by the constraint $\sum_i m_i = M$. The values of the intermediate magnetic quantum numbers $\overline{M}_i$ can be deduced from the magnetic quantum numbers of the involved single spins, i.e. $\overline{M}_1 = m_1 + m_2$ and $\overline{M}_2 = \overline{M}_1 + m_3$.

Following Equations (26) and (61), performing the π-rotation described by the operator $\underset{\sim}{G}(3\,4\,1\,2)$ results in the expression

$$\underset{\sim}{G}(3\,4\,1\,2)\ |s_1 s_2 \overline{S}_1 s_3 \overline{S}_2 s_4 SM\rangle = \sum_{\sum_i m_i = M} C^{s_1 s_2 \overline{S}_1}_{m_1 m_2 \overline{M}_1} \cdot C^{\overline{S}_1 s_3 \overline{S}_2}_{\overline{M}_1 m_3 \overline{M}_2} \cdot C^{\overline{S}_2 s_4 S}_{\overline{M}_2 m_4 M} \times |m_3 m_4 m_1 m_2\rangle. \tag{62}$$

Due to the performed permutation on the product states the resulting state cannot easily be represented as a vector-coupling state belonging to the former coupling scheme given by the successive addition of spin operators: $\underset{\sim}{\mathbf{s}}(1) + \underset{\sim}{\mathbf{s}}(2) = \underset{\sim}{\overline{\mathbf{S}}}(1)$, $\underset{\sim}{\overline{\mathbf{S}}}(1) + \underset{\sim}{\mathbf{s}}(3) = \underset{\sim}{\overline{\mathbf{S}}}(2)$, and $\underset{\sim}{\overline{\mathbf{S}}}(2) + \underset{\sim}{\mathbf{s}}(4) = \mathbf{S}$.

At this point, it becomes obvious that the operator $\underset{\sim}{G}$ is inducing a transition from the coupling scheme, according to which the basis states have initially been constructed, to another one. A proper re-labeling of the summation indices in the sum of Equation (62) with respect to a point-group operation R^{-1}, i.e. a $(-\pi)$-rotation around the central C_2-axis, reveals the resulting coupling scheme in which $\underset{\sim}{G}(3\,4\,1\,2)|s_1 s_2 \overline{S}_1 s_3 \overline{S}_2 s_4 SM\rangle$ can be represented as a vector-coupling state [34]. In this special case one finds that $\underset{\sim}{G}(3\,4\,1\,2)$ is inducing a transition to a coupling scheme given by $\underset{\sim}{\mathbf{s}}(3) + \underset{\sim}{\mathbf{s}}(4) = \underset{\sim}{\overline{\mathbf{S}}}(1')$, $\underset{\sim}{\overline{\mathbf{S}}}(1') + \underset{\sim}{\mathbf{s}}(1) = \underset{\sim}{\overline{\mathbf{S}}}(2')$, and $\underset{\sim}{\overline{\mathbf{S}}}(2') + \underset{\sim}{\mathbf{s}}(2) = \mathbf{S}$. As a shorthand notation one can write

$$\left|s_1 s_2 \overline{S}_1 s_3 \overline{S}_2 s_4 SM\right\rangle \xrightarrow{\underset{\sim}{G}(3\,4\,1\,2)} \left|s_3 s_4 \overline{S}_{1'} s_1 \overline{S}_{2'} s_2 SM\right\rangle,$$

with the limitation that this expression does not give the concrete values of the appearing quantum numbers of the states. Nevertheless, it illustrates the transition between vector-coupling states of different and thus independent coupling schemes.

Table 2. Classes of the D_4 point group with corresponding operators for the spin square. The symmetry (i.e. permutation) operations are defined as in the following example: $\underset{\sim}{G}(2\,3\,4\,1)$ means that spin 2 moves to position 1, spin 3 to position 2, spin 4 to position 3, and spin 1 to position 4.

	Classes				
D_4	E	C_2	$2C_4$	$2C_2'$	$2C_2''$
op's	$\underset{\sim}{G}(1\,2\,3\,4)$	$\underset{\sim}{G}(3\,4\,1\,2)$	$\underset{\sim}{G}(4\,1\,2\,3)$ $\underset{\sim}{G}(2\,3\,4\,1)$	$\underset{\sim}{G}(2\,1\,4\,3)$ $\underset{\sim}{G}(4\,3\,2\,1)$	$\underset{\sim}{G}(1\,4\,3\,2)$ $\underset{\sim}{G}(3\,2\,1\,4)$

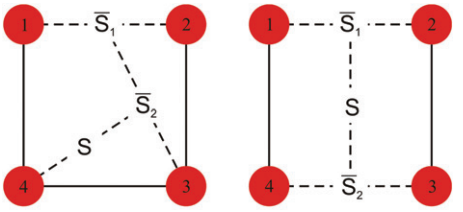

Figure 18. [Colour online] Visualization of two possible couplings for the square: successive coupling scheme (left-hand side) and pairwise coupling scheme (right-hand side).

Following Equation (28) the action of the π-rotation on a vector-coupling state of the chosen form results in

$$\underset{\sim}{G}(3\,4\,1\,2)\left|s_1 s_2 \overline{S}_1 s_3 \overline{S}_2 s_4 SM\right\rangle = \sum_{\overline{S}_1', \overline{S}_2'} \delta_{\overline{S}_1, \overline{S}_{1'}} \delta_{\overline{S}_2, \overline{S}_{2'}} \left|s_1 s_2 \overline{S}_1' s_3 \overline{S}_2' s_4 SM\right\rangle \times \left\langle s_1 s_2 \overline{S}_1' s_3 \overline{S}_2' s_4 SM \middle| s_3 s_4 \overline{S}_{1'} s_1 \overline{S}_{2'} s_2 SM\right\rangle. \quad (63)$$

As mentioned in Section 2.4 the main task when calculating the action of a point-group operation on a vector-coupling state is the determination of the general recoupling coefficients connecting states of the initial and the resulting coupling scheme. Generating a formula for general recoupling coefficients can only be performed in a rather advanced procedure (see Appendix B).

Regarding the recoupling coefficients that appear when performing point-group operations, a very helpful simplification shall be mentioned here. From Equation (62) it can be seen that the action of the operator $\underset{\sim}{G}(3\,4\,1\,2)$ on the product states prevents the re-expression of the resulting linear combination of product states as a simple vector-coupling state belonging to the initial coupling scheme. However, the choice of the coupling scheme according to which the initial basis was constructed is somewhat arbitrary. In order to minimize the computational effort, which is directly related to the number of states with non-zero recoupling coefficient in Equation (63), one has to choose a non-successive coupling scheme. A favorable coupling scheme of this kind is shown in Figure 18. This scheme is referred to as a pairwise coupling scheme and the basis states look like $|s_1 s_2 \overline{S}_1 s_3 s_4 \overline{S}_2 SM\rangle$. The π-rotation around the central C_2-axis of the square now induces a transition that can be symbolized by

$$\left|s_1 s_2 \overline{S}_1 s_3 s_4 \overline{S}_2 SM\right\rangle \xrightarrow{\underset{\sim}{G}(3\,4\,1\,2)} \left|s_3 s_4 \overline{S}_{1'} s_1 s_2 \overline{S}_{2'} SM\right\rangle$$

and leads according to Equation (27) to a recoupling coefficient of the form

$$\left\langle s_1 s_2 \overline{S}_1 s_3 s_4 \overline{S}_2 SM \middle| s_3 s_4 \overline{S}_{1'} s_1 s_2 \overline{S}_{2'} SM\right\rangle.$$

Now, the calculation of a formula for this recoupling coefficient is trivial since the intermediate spin operators of the initial and the resulting coupling scheme are mutually the same, i.e. $\underset{\sim}{\overline{\mathbf{S}}}(1') = \underset{\sim}{\overline{\mathbf{S}}}(2)$ and $\underset{\sim}{\overline{\mathbf{S}}}(2') = \underset{\sim}{\overline{\mathbf{S}}}(1)$. Unfolding $|s_3 s_4 (\overline{S}_{1'} = \overline{S}_2) s_1 s_2 (\overline{S}_{2'} = \overline{S}_1) SM\rangle$ into a linear combination of product states in analogy to Equation (61) leads to

$$\left|s_3 s_4 \overline{S}_2 s_1 s_2 \overline{S}_1 SM\right\rangle = \sum_{\sum_i m_i = M} C^{s_3 s_4 \overline{S}_2}_{m_3 m_4 \overline{M}_2} \cdot C^{s_1 s_2 \overline{S}_1}_{m_1 m_2 \overline{M}_1} \cdot C^{\overline{S}_2\, \overline{S}_1\, S}_{\overline{M}_2\, \overline{M}_1\, M} \times \left|m_1 m_2 m_3 m_4\right\rangle.$$

In order to convert the Clebsch–Gordan coefficients to a form that appears when unfolding states of the form $|s_1 s_2 \overline{S}_1 s_3 s_4 \overline{S}_2 SM\rangle$ one simply has to use the symmetry property of the Clebsch–Gordan coefficients from Equation (35). This leads to

$$C^{\overline{S}_2\, \overline{S}_1\, S}_{\overline{M}_2\, \overline{M}_1\, M} = (-1)^{\overline{S}_1 + \overline{S}_2 - S} C^{\overline{S}_1\, \overline{S}_2\, S}_{\overline{M}_1\, \overline{M}_2\, M},$$

and thus an expression for the recoupling coefficient is obtained which only contains one simple phase factor:

$$\left\langle s_1 s_2 \overline{S}_1 s_3 s_4 \overline{S}_2 SM \middle| s_3 s_4 \overline{S}_{1'} s_1 s_2 \overline{S}_{2'} SM \right\rangle = (-1)^{\overline{S}_1 + \overline{S}_2 - S}.$$

The action of the operator performing a π-rotation on a state belonging to the pairwise coupling scheme mentioned above therefore directly results in a state belonging to the same coupling scheme with an attached phase factor. Thus, it has been shown that with a cleverly chosen coupling scheme the computational effort that is required for the calculation of symmetrized basis states according to Equation (25) can be minimized. The graphical visualization of possible coupling schemes in a square shown in Figure 18 makes it obvious that one will find a simple recoupling formula depending only on phase factors whenever one can find a coupling scheme that is invariant under the performed symmetry operation [34]. Since one has to sum over all symmetry operations of the group in order to construct symmetrized basis states of a given irreducible representation (see Equation (25)), the underlying coupling scheme should be chosen in such a way as to simplify all or at least most of the resulting recoupling coefficients. This means that the coupling scheme should be invariant under all or at least most of the symmetry operations.

However, one will not always be able to find a coupling scheme that simplifies the calculation of the recoupling coefficients as shown above. Especially if the system under consideration is exhibiting three-fold symmetry axes, such a procedure turns out to be impossible by means of a pairwise coupling scheme. In this case a generalization of finding a recoupling formula independent of the choice of the coupling scheme becomes necessary.

A.6. *Computational effects of the choice of the coupling scheme*

The computational realization of the theoretical background presented in this work has been a central task. The performed calculations would not have been possible without developing a highly parallelized computer program that is well adapted to use in a high performance computing environment. In this section some remarks on the computational effects of the choice of the underlying coupling scheme shall be given. In general, as long as a proper scaling is achieved the most intuitive way to speed up calculations using high performance computers is to distribute calculations among many processing units. Nevertheless, as will be seen below the right choice of initial parameters like the coupling scheme can help to ease the problem of calculating energy spectra and thermodynamic properties of magnetic molecules.

Since several terms appear in this section which might be unknown to the reader, their particular meaning as well as related aspects shall be discussed first. The term *computation time* refers to the cumulative time that is needed in order to perform a certain number of floating point operations (FLOPs). The *execution time* refers to the runtime of the considered part of the program. Assuming a parallel execution of the program with optimal performance, the computation time remains unchanged although the operations are performed in parallel. A reduction of the computation time can be achieved by reducing the number of FLOPs that have to be performed. In contrast to this, the execution time usually decreases with increasing number of processing units. The change of the execution time as a function of the used processing units is called *scaling behavior*. It is referred to as optimal if the execution time is divided by 2 whenever the number of used processing units is doubled. The *speed up* S_p using p processing units is defined as

$$S_p = \frac{T_1}{T_p}, \tag{64}$$

where T_1 and T_p refer to the execution times of the sequential and the parallelized algorithm, respectively. An optimal speed up corresponds to $S_p = p$. The optimal speed up can be achieved if the whole source code can be parallelized without dependencies between the operations which are executed in parallel. Practically, sequential regions and communication between the processing units often limit the speed up to a value that is lower than the number of processing units used.

In general, the computational realization of the presented framework can be divided into two completely independent parts. On the one hand a matrix representation of the Hamiltonian is set up

with the help of the irreducible tensor operator approach. On the other hand this matrix or independent blocks of it are diagonalized, i.e. the eigenvalues and eigenvectors are determined numerically.

If point-group symmetries are used, a very decisive role concerning the computation time is played by the construction of symmetrized basis states. These functions appear as linear combinations of the initial basis states. The weight of the states that are included in these linear combinations is determined by general recoupling coefficients. If a coupling scheme can be found that is invariant under all point-group operations, the number of states that contribute to a linear combination representing a symmetrized basis state is minimized. As already mentioned, a reduction of computation time is achieved by choosing a coupling scheme that minimizes the number of appearing summation indices and Wigner-6J symbols.

The construction of symmetrized basis states plays an important role for extending the limits of numerical exact diagonalization with the help of the concepts presented in this work. Whenever the dimensions of the appearing matrices are to be reduced by the incorporation of point-group symmetries, a certain amount of additional computation time has to be spent on the construction of symmetrized basis states. Since the construction procedure cannot easily be parallelized, the use of more processing units within this particular region does not always lead to the desired reduction of execution time. In any case, one has to ensure that the recoupling formulas, which determine the number of performed FLOPs, are the simplest in order to reduce computation time. As already mentioned, this can be achieved by choosing a coupling scheme that is invariant under the operations of the assumed point-group. The resulting recoupling formulas do then not contain Wigner symbols and are optimal.

In Figure 19 the execution times for the determination of the energy eigenvalues of a cuboctahedron with $s=3/2$ in the subspace $\mathcal{H}(S=0,\ M=0,\ A_1)$ are shown in dependence on the chosen coupling scheme. The used point-group symmetry was D_2 and execution times are given for the choice of a completely invariant and a non-invariant coupling scheme, respectively. Comparing the scaling behavior, one can see that the performance of both calculations is limited by the construction of the symmetrized basis states. Furthermore, it becomes obvious that the set up of the matrices is heavily influenced by the particular form of the symmetrized basis states. In the case of the non-invariant coupling scheme the set up of the matrix has been much slower than in the case of the invariant coupling scheme because the symmetrized basis states involve more states of the initial (vector-coupling) basis.

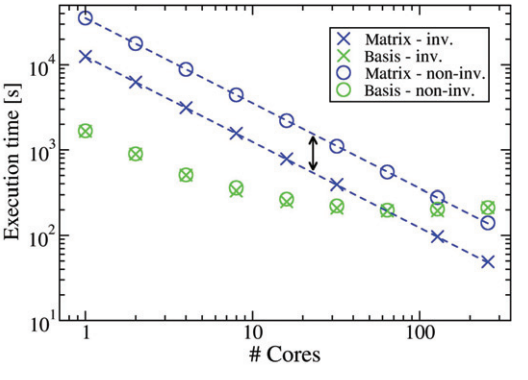

Figure 19. [Colour online] Scaling of OpenMP parallelized regions. Exemplary calculations have been performed using different coupling schemes (cuboctahedron $s=3/2$, D_2, $\mathcal{H}(S=0,\ M=0,\ A_1)$). The crosses refer to an invariant coupling scheme while the circles refer to a non-invariant coupling scheme. The black arrow indicates the different execution times for the set up of the matrices and the dashed lines show the optimal scaling behavior.

B. The calculation of general recoupling coefficients

In this section graph-theoretical considerations are presented that allow us to determine the action of point-group operations on vector-coupling states. It is shown how a general recoupling formula can be developed from mapping general Wigner coefficients on binary trees or Yutsis graphs.

In general, the problem of calculating recoupling coefficients has to be divided into two parts. The first part is the generation of a formula that describes the transition between two different coupling schemes. The second – and much easier – part is the evaluation of a given formula using a specific set of quantum numbers [42]. This section is exclusively focused on the first part, i.e. the generation of a recoupling formula that links different coupling schemes in systems with an arbitrary number of participating spins which turns out to be more difficult.

B.1. *Binary trees*

In the literature one can find successful implementations that deal with the generation of formulas for general recoupling coefficients which only involve a series of phase factors and Wigner-6J symbols [45–47]. The most intuitive way of generating a recoupling formula is to operate on so-called binary trees [116–118]. The correspondence between a binary tree and a given coupling scheme is rather obvious. Each coupling of two spins s_a and s_b to a compound spin s_c forms a triad that corresponds to an elementary binary tree shown in Figure 20. This tree is composed of only three angular momenta and can simultaneously be seen as representing a Clebsch–Gordan coefficient. From such elementary trees a binary tree can be built up step-by-step that represents the chosen coupling scheme. The tree constructed this way then contains all Clebsch–Gordan coefficients that result from the decomposition of a vector-coupling state belonging to the particular coupling scheme into product states (cf. Equations (43) and (44)).

Operating on binary trees in order to generate a formula for a general recoupling coefficient directly leads to the procedure that limits the resulting expressions to 6J symbols. Here, the generation of a formula for the recoupling coefficient $\langle s_1 s_2 \overline{S}_1 s_3 \overline{S}_2 s_4 SM | s_3 s_4 \overline{S}_{1'} s_1 \overline{S}_{2'} s_2 SM \rangle$, that appears in Equation (63), shall be presented. In this case, generating a recoupling formula corresponds to finding a transition between the binary trees that are shown in Figure 21. In other words, one transforms the set of Clebsch–Gordan coefficients that is represented by the initial tree (left-hand side of Figure 21) to the set that is represented by the targeted tree (right-hand side of Figure 21).

Following the usual graph-theoretical name convention the single-spin quantum numbers are referred to as *leaf nodes* while the intermediate spin quantum numbers are called *coupled nodes*. The total-spin quantum number appears as a coupled node of a special kind and is called *root*.

There are in general two types of operations that have to be performed in a certain manner in order to yield the desired form of the recoupling coefficient. These operations are shown in Figure 22 and are called an *exchange* operation and a *flop* operation. Both operations are only performed on subtrees of the initial tree, thus only leading to changes in the particular subtree while leaving the rest of the tree unchanged. With every operation a certain contribution to the recoupling formula is obtained.

An exchange operation refers to a recoupling coefficient that appears when considering the recoupling of two spins s_a and s_b within a single triad. Obviously, the only way of recoupling these

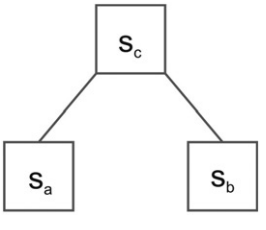

Figure 20. Binary tree that corresponds to a single coupling of two spins s_a and s_b to a compound spin s_c.

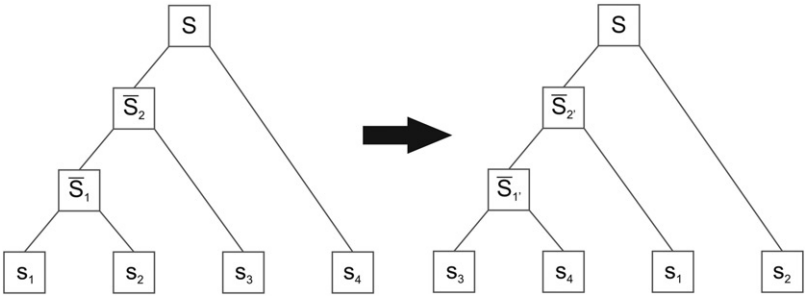

Figure 21. Transition between two binary trees that has to be performed in order to calculate the recoupling coefficient $\langle s_1 s_2 \overline{S}_1 s_3 \overline{S}_2 s_4 SM | s_3 s_4 \overline{S}_{1'} s_1 \overline{S}_{2'} s_2 SM \rangle$.

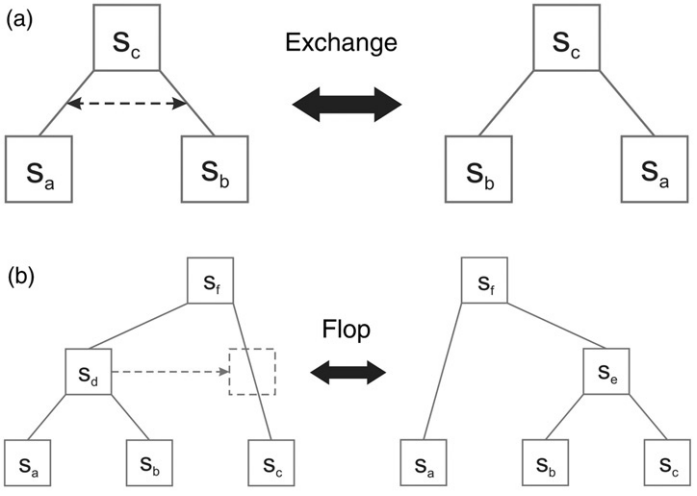

Figure 22. Operations on a binary tree that lead to a formula for a general recoupling coefficient.

spins is to perform an exchange between them. The effect of this operation can easily be derived from unfolding the vector-coupling states $|s_a s_b s_c\rangle$ and $|s_b s_a s_c\rangle$ in terms of product states according to Equation (34). A state of the form $|s_a s_b s_c\rangle$ can be written as a state of the form $|s_b s_a s_c\rangle$ by using the symmetry property of the Clebsch–Gordan coefficients from Equation (35), leading to a recoupling coefficient

$$\langle s_a s_b s_c | s_b s_a s_c \rangle = (-1)^{\pm(s_a + s_b - s_c)}. \tag{65}$$

In analogy, a flop operation refers to the recoupling of three spins s_a, s_b, and s_c. Denoting the intermediate spin by s_d and the total spin by s_f, a successive coupling scheme would lead to states that can be written as $|s_a s_b s_d s_c s_f\rangle$. However, a second coupling scheme can be designed that results in states of the form $|s_a s_b s_c s_e s_f\rangle$. By definition a transition between these coupling schemes is described by a Wigner-6J symbol resulting in

$$\begin{aligned} \langle s_a s_b s_d s_c s_f | s_a s_b s_c s_e s_f \rangle = (-1)^{\pm(s_a + s_b + s_c + s_f)} \sqrt{(2s_d + 1)(2s_e + 1)} \\ \times \begin{Bmatrix} s_a & s_b & s_d \\ s_c & s_f & s_e \end{Bmatrix}. \end{aligned} \tag{66}$$

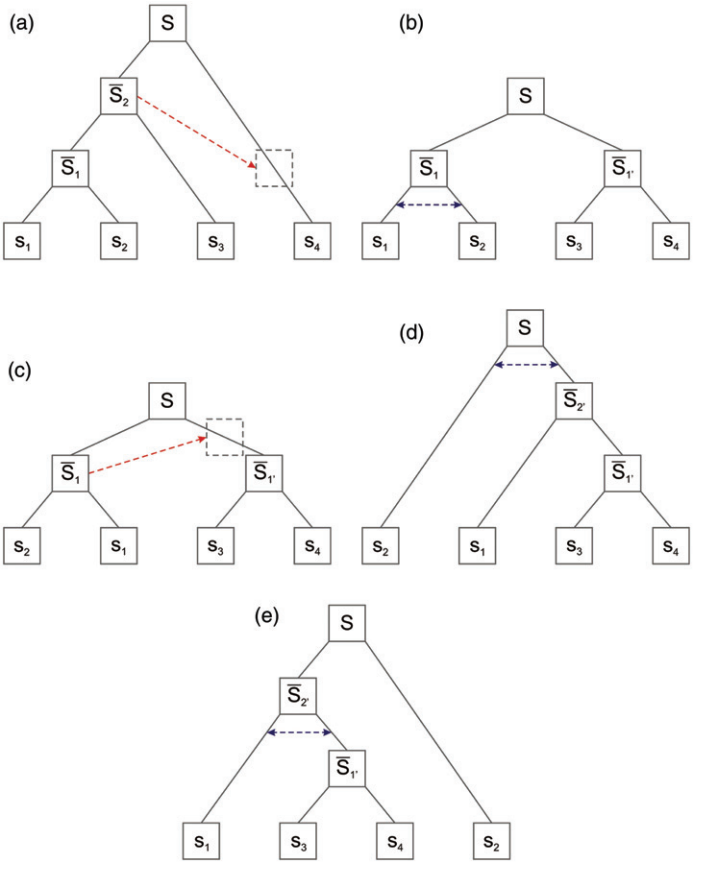

Figure 23. [Colour online] Sequence of operations leading to the recoupling coefficient $\langle s_1 s_2 \overline{S}_1 s_3 \overline{S}_2 s_4 SM | s_3 s_4 \overline{S}_{1'} s_1 \overline{S}_{2'} s_2 SM \rangle$. Figures (b), (d), and (e) show exchange operations. In (a) and (d) flop operations are shown.

It has to be mentioned that the flop operation shown in Figure 22(b) was assumed to create a node, i.e. a spin quantum number that already exists in the targeted coupling scheme, namely $s_{e'}$. Whenever a flop operation is performed that creates a node which is unknown in the targeted coupling scheme, a summation variable has to be introduced within the resulting contribution to the recoupling formula. This summation variable is completely determined by the symmetry of the appearing Wigner-6J coefficient. The contribution resulting from a flop operation that creates an unknown node $s_{e'}$ within the binary tree would look like

$$(-1)^{\pm(s_a+s_b+s_c+s_f)} \sum_{s_{e'}} \sqrt{(2s_d+1)(2s_{e'}+1)} \times \begin{Bmatrix} s_a & s_b & s_d \\ s_c & s_f & s_{e'} \end{Bmatrix}.$$

The desired formula for the recoupling coefficient from Equation (63) is now obtained by performing a proper sequence of exchange and flop operations. This sequence is displayed in detail in Figure 23. It is not the only possible sequence of operations on the binary tree that leads to a

recoupling formula for the discussed transition. However, in this simple case the displayed sequence leads to an optimal formula minimizing the number of resulting Wigner-6J symbols.

The result of the operations then reads

$$\langle s_1 s_2 \overline{S}_1 s_3 \overline{S}_2 s_4 SM | s_3 s_4 \overline{S}_{1'} s_1 \overline{S}_{2'} s_2 SM \rangle = \sqrt{(2\overline{S}_{1'}+1)(2\overline{S}_2+1)(2\overline{S}_1+1)(2\overline{S}_{2'}+1)} \times (-1)^{s_1+s_2+s_3+s_4+3S} \begin{Bmatrix} \overline{S}_1 & s_3 & \overline{S}_2 \\ s_4 & S & \overline{S}_{1'} \end{Bmatrix} \begin{Bmatrix} s_2 & s_1 & \overline{S}_1 \\ \overline{S}_{1'} & S & \overline{S}_{2'} \end{Bmatrix}. \quad (67)$$

This simple form was only reached because the flop operations shown in Figures 23(a) and 23(c) create nodes that already exist in the final coupling scheme, i.e. $\overline{S}_{1'}$ and $\overline{S}_{2'}$.

As long as such simple recoupling coefficients are considered, the process of determining a proper sequence leading from the initial coupling scheme to the targeted one can be easily done by hand and does not need any automatization. Nevertheless, more sophisticated problems result in transitions between binary trees that cannot easily be treated. Then, it becomes necessary to set up an algorithm that automatically creates a proper – ideally optimal – sequence. Regarding binary trees, known implementations [116,117] of such algorithms can be seen as trial-and-error procedures.

By performing a subsequence of operations, initially containing only one exchange or flop operation, one tries to find a tree containing a node that is known in the targeted coupling scheme. Whenever it is impossible to find such a tree with the given number of operations in the subsequence, the number of considered operations is increased, i.e. the subsequence is extended. A successful implementation of this procedure leads to a stepwise creation of the targeted tree in which each step is guaranteed to be performed with the smallest (overall) number of exchange and flop operations. However, the minimization of the number of operations within the performed subsequences does not ensure that the resulting recoupling formula is optimal. In general, a recoupling formula is optimal if the number of occurring summation variables and Wigner-6J coefficients is minimal. Since summation variables and 6J symbols are only introduced by flop operations, generating an improved recoupling formula directly corresponds to reducing the number of performed flops.

B.2. *Graph-theoretical solution – Yutsis graphs*

As shown in the last section, operating on binary trees in order to generate a recoupling formula involving only phase factors, square roots, and Wigner-6J symbols already leads to a simple and successful procedure. However, the process of determining an optimized sequence of operations remains concealed. In order to improve this process and thus improve the recoupling formula, ideas resulting from more advanced graph-theoretical considerations can be applied. In Refs. [41,119–121] the problem of generating a recoupling formula was solved with the help of *Yutsis graphs*. This procedure, providing a technically more difficult, but at the same time theoretically more transparent way of generating an improved recoupling formula, shall be reviewed in this section.

The creation of Yutsis graphs is a straightforward task starting from the background given in Appendix B.1. In order to understand how these graphs evolve, an explanation of how to construct a Yutsis graph shall be given here. Additionally, the reduction of such a graph leading to an improved recoupling formula will be discussed briefly. The interested reader will find a deeper and more theoretical investigation of general features of Yutsis graphs in the literature [115,122].

As already discussed in Section A.1 an expression for a recoupling coefficient in terms of Clebsch–Gordan coefficients or Wigner-3J symbols can be found by decomposing the bra and the ket states into sums of product states. In order to clarify this procedure, the recoupling coefficient $\langle s_1 s_2 \overline{S}_1 s_3 \overline{S}_2 s_4 SM | s_3 s_4 \overline{S}_{1'} s_1 \overline{S}_{2'} s_2 SM \rangle$ shall be discussed in detail as an example. The decomposition of $|s_1 s_2 \overline{S}_1 s_3 \overline{S}_2 s_4 SM\rangle$ was already done in Appendix A.5 and is given in terms of Clebsch–Gordan coefficients in Equation (61). Replacing the Clebsch–Gordan coefficients by

Wigner-3J symbols yields

$$|s_1 s_2 \overline{S}_1 s_3 \overline{S}_2 s_4 SM\rangle = \sum_{\{m_i\}} \left\{ \sum_{\{\overline{M}_i\}} C(\alpha) \begin{pmatrix} s_1 & s_2 & \overline{S}_1 \\ m_1 & m_2 & -\overline{M}_1 \end{pmatrix} \begin{pmatrix} \overline{S}_1 & s_3 & \overline{S}_2 \\ \overline{M}_1 & m_3 & -\overline{M}_2 \end{pmatrix} \times \begin{pmatrix} \overline{S}_2 & s_4 & S \\ \overline{M}_2 & m_4 & -M \end{pmatrix} \right\} |m_1 m_2 m_3 m_4\rangle, \tag{68}$$

where $C(\alpha)$ contains the square roots as well as the phase factors that appear when transforming Clebsch–Gordan coefficients into Wigner symbols. The multiple sums run over all single-spin magnetic quantum numbers m_i and the magnetic quantum numbers $\overline{M}_i$ of the intermediate spins. The curly brackets are reminiscent of a generalized Wigner coefficient. The same decomposition yields for the ket state

$$|s_3 s_4 \overline{S}_{1'} s_1 \overline{S}_{2'} s_2 SM\rangle = \sum_{\{m_i\}} \left\{ \sum_{\{\overline{M}_{i'}\}} C(\beta) \begin{pmatrix} s_3 & s_4 & \overline{S}_{1'} \\ m_3 & m_4 & -\overline{M}_{1'} \end{pmatrix} \begin{pmatrix} \overline{S}_{1'} & s_1 & \overline{S}_{2'} \\ \overline{M}_{1'} & m_1 & -\overline{M}_{2'} \end{pmatrix} \times \begin{pmatrix} \overline{S}_{2'} & s_2 & S \\ \overline{M}_{2'} & m_2 & -M \end{pmatrix} \right\} |m_1 m_2 m_3 m_4\rangle. \tag{69}$$

From Equations (68) and (69) one immediately finds the following expression for the recoupling coefficient:

$$\begin{aligned} \langle s_1 s_2 \overline{S}_1 s_3 \overline{S}_2 s_4 SM | s_3 s_4 \overline{S}_{1'} s_1 \overline{S}_{2'} s_2 SM\rangle &= \sum_{\{m_i\},\{m_i'\}} P^{\alpha}(\{m_i\}) \cdot P^{\beta}(\{m_i'\}) \\ &\quad \times \langle m_1 m_2 m_3 m_4 | m_1' m_2' m_3' m_4'\rangle \\ &= \sum_{\{m_i\},\{m_i'\}} \delta_{\{m_i\},\{m_i'\}} P^{\alpha}(\{m_i\}) \cdot P^{\beta}(\{m_i'\}). \end{aligned} \tag{70}$$

The abbreviations P^{α} and P^{β} stand for the generalized Wigner coefficients that depend on the quantum numbers of the underlying coupling schemes which the sets α and β refer to. The derived expression for the recoupling coefficient in Equation (70) still involve magnetic quantum numbers. Since a recoupling coefficient is in general independent of any magnetic quantum number, a simplification can be found that only involves spin quantum numbers. Such a simplification was already found in the former section with the help of binary trees and will now be discussed on the basis of Yutsis graphs.

The main idea of generating a recoupling formula with the help of Yutsis graphs is – in a first step – to set up a graphical representation of generalized Wigner coefficients as they appear in Equations (68) and (69). Afterwards, these graphs are joined in order to build up a Yutsis graph that represents the recoupling coefficient. A simplification of the constructed Yutsis graph according to special operations then leads to the desired formula that is independent of magnetic quantum numbers.

The building blocks of Yutsis graphs are diagrammatic representations of Wigner-3J symbols. Figure 24 shows two diagrammatic representations of the same Wigner-3J symbol

$$\begin{pmatrix} s_a & s_b & s_c \\ m_a & m_b & m_c \end{pmatrix}.$$

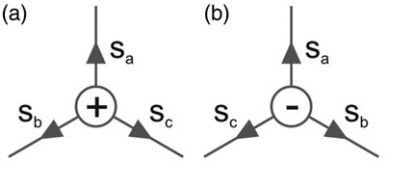

Figure 24. Two diagrams of the same Wigner-3J symbol with different sign of the nodes. The sign is related to the cyclic ordering of the lines.

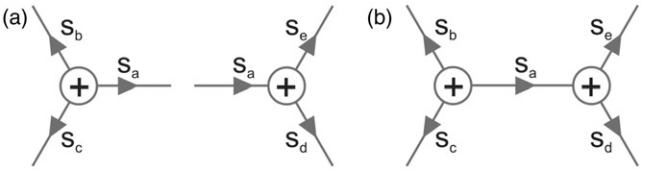

Figure 25. Contracting the open ends of two lines labeled by s_a that leads to a summation over the magnetic quantum number m_a of the joined lines.

Such a representation consists of three lines and one node. With every spin quantum number in the Wigner symbol a line is identified. The three lines are connected by the node. The node is labeled with a (+) or (−) sign while the lines are characterized by the direction they are pointing in. The (−) sign denotes a clockwise orientation of the spin quantum numbers within the corresponding Wigner-3J symbol (cf. Figure 24(b)) whereas the (+) sign indicates an anticlockwise ordering (cf. Figure 24(a)). The free ends of the lines represent the projections of the spin quantum numbers, i.e. the magnetic quantum numbers m_a, m_b, and m_c. If a line leads away from the node, the corresponding magnetic quantum number appears with a positive sign in the Wigner symbol, whereas it appears with a negative sign if the line is directed towards the node.

It is obvious that any operation that changes the diagrams of the Wigner symbol in Figure 24 will lead to a Wigner symbol that differs from the original one. Changing the sign of the node or simultaneously changing the directions of all lines results in a factor that can be obtained from the symmetry properties of the Wigner-3J symbols described in Section A.1. The change of the sign corresponds to an uneven permutation of spins within the Wigner-3J symbol (cf. Equation (37)) while the change of all directions of the lines corresponds to multiplying the lower row of the original Wigner-3J symbol by −1 (cf. Equation (38)). Both operations result in a phase factor of $(-1)^{s_a+s_b+s_c}$ whereas any rotation of the diagram has no effect on the Wigner-3J symbol since the ordering remains unchanged.

In order to construct a graph that represents a generalized Wigner coefficient, another operation has to be introduced. As shown in Figure 25, the diagrams of two Wigner symbols can be contracted if two lines exist that are labeled by the same quantum number and point into the same direction. The resulting graph then represents a summation over the corresponding magnetic quantum number given by

$$\sum_{m_a} \begin{pmatrix} s_a & s_b & s_c \\ m_a & m_b & m_c \end{pmatrix} \begin{pmatrix} s_a & s_d & s_e \\ -m_a & m_d & m_e \end{pmatrix}. \tag{71}$$

Figures 26(a) and 26(b) show graphical representations of the generalized Wigner coefficients as found in Equations (68) and (69). They are easily constructed following the conventions introduced above.

The arrangement of the diagrams representing generalized Wigner coefficients is chosen in such a way as to ease the contraction of both graphs and was proposed in Ref. [115]. The graph representing the left-hand side of the recoupling coefficient contains only negative nodes with the spins being ordered clockwise around these nodes. In the graph belonging to the right-hand side of the recoupling coefficient the spins are ordered anticlockwise around the nodes that exclusively have a positive sign. The directions of the lines are chosen in Figure 26(a) so as to match the conventional form of Wigner-3J symbols in generalized Wigner coefficients. In Figure 26(b) they are chosen in the opposite direction in order to compensate the phase factors that result from the positive signs of the nodes.

In Figure 26(c) both diagrams of the Wigner coefficients are contracted. The contraction corresponds to a summation over the magnetic quantum numbers m_i, $i = 1, \ldots, 4$, as well as over M. The summations over the magnetic quantum numbers of the intermediate spins $\{\overline{M}_i\}$ and $\{\overline{M}_{i'}\}$ has already been included in the representations of the coupling schemes in Figures 26(a) and 26(b),

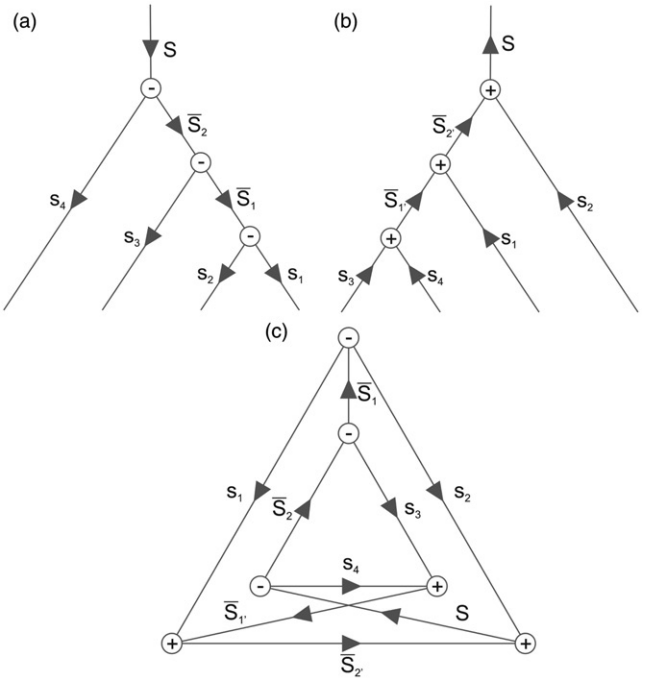

Figure 26. Graphical representation of the generalized Wigner coefficients for the coupling schemes contained in the recoupling coefficient $\langle s_1 s_2 \overline{S}_1 s_3 \overline{S}_2 s_4 SM | s_3 s_4 \overline{S}_{1'} s_1 \overline{S}_{2'} s_2 SM \rangle$ as well as the resulting Yutsis graph. (a) Shows the initial coupling scheme, (b) the targeted coupling scheme, and (c) the resulting Yutsis graph.

respectively. The resulting Yutsis graph then represents – apart from square roots and phase factors – the recoupling coefficient that is given in Equation (70).

In general, a recoupling coefficient is equal to a Yutsis graph, which is constructed according to the above rules, times an additional factor [115]. This factor contains phase factors and square roots that emerge from expressing Clebsch–Gordan coefficients in terms of Wigner-3J symbols and additional contributions from initializing the graphical representation of the general Wigner coefficients (see Figures 26(a) and 26(b)). It can be written as

$$(-1)^{2\left(S+\sum_{i=1}^{N-2}\overline{S}_{i'}+\mathcal{S}\right)}\left[\prod_{i=1}^{N-2}\left(2\overline{S}_i+1\right)\left(2\overline{S}_{i'}+1\right)\right]^{1/2}. \tag{72}$$

Here N is the number of single spins in the system under consideration and the sum in the exponent is running over all intermediate spin quantum numbers $\overline{S}_{i'}$ of the targeted coupling scheme. $\mathcal{S}$ represents the sum of the so-called *first coupled angular momenta*, i.e. the sum of those spins that appear in the bra-ket notation of the recoupling coefficient in the first position of each coupling triad. In the case of the recoupling coefficient $\langle s_1 s_2 \overline{S}_1 s_3 \overline{S}_2 s_4 SM | s_3 s_4 \overline{S}_{1'} s_1 \overline{S}_{2'} s_2 SM \rangle$, the sum of the first coupled angular momenta is given by

$$\mathcal{S} = s_1 + \overline{S}_1 + \overline{S}_2 + s_3 + \overline{S}_{1'} + \overline{S}_{2'}.$$

The formula for the recoupling coefficient is now obtained by a successive reduction of *cycles* that appear in the graph. A cycle refers to a loop that connects a certain number of nodes.

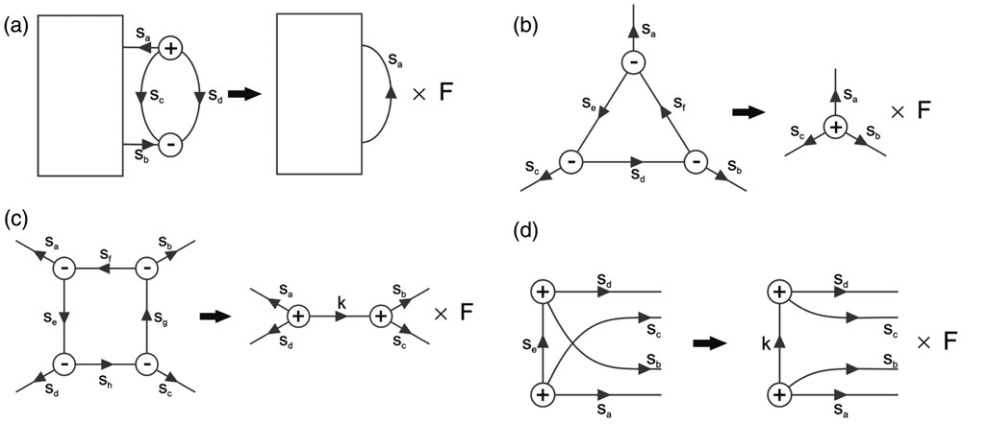

Figure 27. Operations on a Yutsis graph and resulting contributions to the recoupling formula. (a), (b), and (c) show the reduction of 2-, 3-, and 4-cycles, respectively. In (d) the action of an interchange operation is shown.

Table 3. Contributions F to the recoupling formula resulting from the reduction of an N-cycle (cf. Figure 27). The case $N>4$ refers to an interchange operation which is used in order to express larger cycles in terms of 2-, 3-, and 4-cycles.

N	F
2	$(2s_a+1)^{-1}\,\delta_{s_a,s_b}$
3	$\begin{Bmatrix} s_a & s_b & s_c \\ s_d & s_e & s_f \end{Bmatrix}$
4	$\sum_k (-1)^{k+s_f-s_h}(2k+1)\begin{Bmatrix} s_a & s_d & k \\ s_h & s_f & s_e \end{Bmatrix}\begin{Bmatrix} s_b & s_c & k \\ s_h & s_f & s_g \end{Bmatrix}$
>4	$\sum_k (-1)^{s_b+s_c+s_e+k}(2k+1)\begin{Bmatrix} s_a & s_b & k \\ s_d & s_c & s_e \end{Bmatrix}$

Depending on the number of connected nodes, different operations exist that reduce the graph. Figure 27 shows the operations leading to a reduction of 2-, 3-, and 4-cycles. Additionally, an interchange operation is shown that can be used in order to express cycles which cannot be reduced immediately, i.e. cycles with more than four nodes, in terms of 2-, 3-, and 4-cycles [41]. The contributions F to the recoupling formula resulting from the shown operations are listed in Table 3. The values for the quantum numbers k related to the re-labeled edges in Figures 27(c) and 27(d) are determined by the symmetry properties of the Wigner-6J symbols within these contributions. Whenever performing reductions on a Yutsis graph, the directions of the edges as well as the signs of the nodes have to be considered carefully. Within the Yutsis graph that is supposed to be reduced these directions and signs eventually have to be changed in order to match the constellation of the edges and the nodes shown in Figure 27. In this process the change of the direction of an edge s, i.e. a contracted line, contributes with $(-1)^{2s}$ to the phase of the recoupling coefficient.

The contributions to the recoupling formula arising from reducing the Yutsis graph according to the above mentioned operations are discussed in detail in Ref. [115] and shall not be further explained here for the sake of brevity.

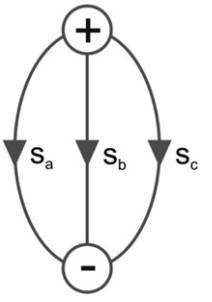

Figure 28. Graphical representation of a triangular delta.

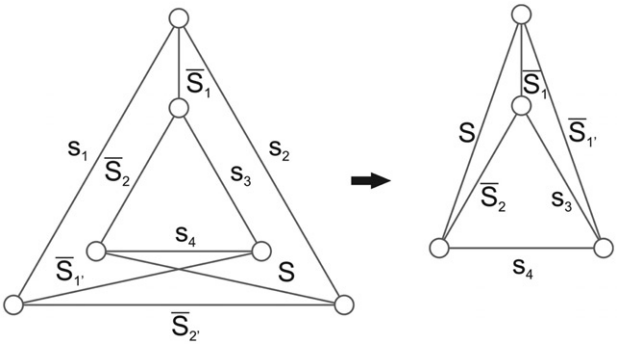

Figure 29. Reduction of the outer triangle of the Yutsis graph from Figure 26(c).

A Yutsis graph is said to be reduced whenever a graphical representation is obtained that corresponds to the one in Figure 28. This representation is called a *triangular delta* and gives a factor 1, if s_a, s_b, and s_c satisfy the triangular condition (Equation (31)), and a factor 0 otherwise [115].

Coming back to the example of calculating the recoupling coefficient $\langle s_1 s_2 \overline{S}_1 s_3 \overline{S}_2 s_4 SM | s_3 s_4 \overline{S}_{1'} s_1 \overline{S}_{2'} s_2 SM \rangle$ that is displayed in Figure 26(c), one immediately finds two 3-cycles which can be reduced in order to generate a recoupling formula: s_1-s_2-$\overline{S}_{2'}$ and s_3-s_4-$\overline{S}_2$. As a result of this reduction, the recoupling formula contains, apart from phase factors and square roots, two Wigner-6J symbols as in Equation (67).

However, as already mentioned in Appendix B.1 there is in general more than one possibility of reducing a graph. Figure 29 shows a possible first step that reduces the outer triangle spanned by the edges s_1, s_2, and $\overline{S}_{2'}$. For the sake of clarity the signs of the nodes as well as the directions of the edges are omitted since they only contribute to the phase of the recoupling coefficient. As one can see after reducing the outer triangle, four different triangles appear. The reduction of each triangle would then lead to a triangular delta and therefore to a completed recoupling formula. These formulas look slightly different but can of course be transformed into each other. One possible expression for the recoupling coefficient is given by

$$\begin{aligned}\langle s_1 s_2 \overline{S}_1 s_3 \overline{S}_2 s_4 SM | s_3 s_4 \overline{S}_{1'} s_1 \overline{S}_{2'} s_2 SM \rangle = (-1)^{-s_1-s_2-s_3-s_4+\overline{S}_1-\overline{S}_{1'}+2\overline{S}_{2'}} \\ \times \sqrt{(2\overline{S}_{1'}+1)(2\overline{S}_{2'}+1)(2\overline{S}_1+1)(2\overline{S}_2+1)} \\ \times \begin{Bmatrix} S & \overline{S}_1 & \overline{S}_{1'} \\ s_1 & \overline{S}_{2'} & s_2 \end{Bmatrix} \begin{Bmatrix} s_4 & S & \overline{S}_2 \\ \overline{S}_1 & s_3 & \overline{S}_{1'} \end{Bmatrix}. \end{aligned} \tag{73}$$

So far, this section has dealt with the construction of a Yutsis graph and those operations that reduce this graph to a triangular delta. In principle, one could generate recoupling formulas and calculate general recoupling coefficients with this information. In the discussed example of Figure 26(c) only triangles appear leading to an easy reduction that contributes two Wigner-6J symbols to the recoupling formula. However, in larger systems with high symmetry often more complicated recoupling coefficients have to be calculated. In order to minimize the computational effort it is desirable to generate a formula that contains as few Wigner-6J symbols and summation indices as possible. Again, they result from triangles, squares, and cycles of higher order.

The most intuitive way of generating an improved recoupling formula is to reduce the smallest cycles first. This idea was implemented in Refs. [41,119,120] and already yields considerably improved formulas in comparison to the use of a trial-and-error technique. However, these formulas can be further improved by using a more sophisticated strategy of reducing cycles [121].

Summarizing this section, one can say that with the help of graph-theoretical methods the effect of general point-group operations on vector-coupling states can be determined. Once this effect is known, the eigenstates of the system under consideration can be labeled with respect to irreducible representations of the point group. This characterization not only reduces the dimensions of the Hamilton matrices saving hardware resources, but it also provides deeper insight into the physics of the system arising from its geometry.